Starvation and ULK1-dependent cycling of mammalian Atg9 between the TGN and endosomes

Andrew R. J. Young[1], Edmond Y. W. Chan[1], Xiao Wen Hu[1], Robert Köchl[1], Samuel G. Crawshaw[2], Stephen High[2], Dale W. Hailey[3], Jennifer Lippincott-Schwartz[3] and Sharon A. Tooze[1,*]

[1]Cancer Research UK London Research Institute, 44 Lincoln's Inn Fields, London, WC2A 3PX, UK
[2]Faculty of Life Sciences, University of Manchester, Smith Building, Oxford Road, Manchester, M13 9PT, UK
[3]NIH / NICHD / CBMB, Bldg 18T Room 101, 9000 Rockville Pike, Bethesda, MD, 20892, USA
*Author for correspondence (e-mail: Sharon.tooze@cancer.org.uk)

Accepted 11 July 2006
Journal of Cell Science 119, 3888-3900 Published by The Company of Biologists 2006
doi:10.1242/jcs.03172

Summary

Autophagy, fundamentally a lysosomal degradation pathway, functions in cells during normal growth and certain pathological conditions, including starvation, to maintain homeostasis. Autophagosomes are formed through a mechanism that is not well understood, despite the identification of many genes required for autophagy. We have studied the mammalian homologue of Atg9p, a multi-spanning transmembrane protein essential in yeast for autophagy, to gain a better understanding of the function of this ubiquitious protein. We show that both the N- and C-termini of mammalian Atg9 (mAtg9) are cytosolic, and predict that mAtg9 spans the membrane six times. We find that mAtg9 is located in the trans-Golgi network and late endosomes and colocalizes with TGN46, the cation-independent mannose-6-phosphate receptor, Rab7 and Rab9. Amino acid starvation or rapamycin treatment, which upregulates autophagy, causes a redistribution of mAtg9 from the TGN to peripheral, endosomal membranes, which are positive for the autophagosomal marker GFP-LC3. siRNA-mediated depletion of the putative mammalian homologue of Atg1p, ULK1, inhibits this starvation-induced redistribution. The redistribution of mAtg9 also requires PI 3-kinase activity, and is reversed after restoration of amino acids. We speculate that starvation-induced autophagy, which requires mAtg9, may rely on an alteration of the steady-state trafficking of mAtg9, in a Atg1-dependent manner.

Supplementary material available online at
http://jcs.biologists.org/cgi/content/full/119/18/3888/DC1

Key words: Autophagy, Golgi, Rab proteins, Intracellular transport, Transmembrane protein

Introduction

During amino acid deprivation cells upregulate autophagy, self-digestion, to maintain their amino acid pools and protein synthesis. Autophagy, required for cell survival under both basal and stress conditions, is involved in the control of embryonic and early postnatal development, neurodegenerative diseases, and tumourigenesis (Klionsky, 2005). Autophagy is executed by autophagosomes (also called autophagic vacuoles, AVs). AVs are double or multiple lamellar vesicles containing sequestered cytosol, including organelles. Newly-formed AVs, or immature autophagosomes (AVis), fuse with vesicles of the endosomal/lysosomal system, becoming degradative AVs (AVds) and autolysosomes. Under starvation conditions, degradation of the AV provides amino acids to allow the cell to maintain protein synthesis.

The source of the AV membranes in mammalian cells is controversial: some studies (Dunn, Jr, 1990; Ericsson, 1969; Novikoff and Shin, 1978; Ueda et al., 1991) have identified endoplasmic reticulum (ER) proteins on the AVi, others detected Golgi membrane proteins (Locke and Sykes, 1975; Yamamoto et al., 1990). The unusual morphological properties of AVs has also led to the hypothesis that these membranes are derived from a unique type of membrane, called a phagophore (Seglen et al., 1990), or isolation membrane (Mizushima et al., 2001). An equivalent structure has been identified in yeast, the pre-autophagosomal structure or PAS (Kim et al., 2002; Suzuki et al., 2001).

Many of the genes now known to be involved in autophagy were originally identified in independent screens for autophagy-defective mutants in *S. cerevisiae* (Thumm et al., 1994; Tsukada and Ohsumi, 1993) and are now called AuTophaGy (ATG) genes (Klionsky et al., 2003). Interestingly, there is only one characterized yeast ATG gene, *ATG9*, which is predicted to encode a transmembrane protein. *ATG9*-deficient yeast had no obvious growth defects on rich media but, like other mutants with a defect in autophagy, exhibited a reduced survival rate and reduced total protein turnover during starvation (Lang et al., 2000; Noda et al., 2000).

As the only transmembrane protein so far required for autophagy in yeast, the intracellular localization of Atg9 has provided information about the origin of the PAS in yeast, and should help identify the origin of the AV membrane in mammalian cells. In growing yeast, Atg9p is found on punctate, peri-vacuolar structures, which did not co-migrate with known markers on a sucrose-density gradient (Noda et al., 2000). Recent data suggests that at least part of this pool is localized on discrete regions of mitochondria (Reggiori et al., 2005). After starvation, Atg9p was found on the PAS and

colocalized with the Atg1p complex (Kim et al., 2002). Interestingly, Atg9p was not found on completed AVs (Noda et al., 2000), and is thought to be recycled from the PAS to peripheral, non-PAS membranes. This recycling was shown to be impaired in ATG1-deficient cells, causing Atg9p to accumulate at the PAS (Reggiori et al., 2004). These data have led to the suggestion that the ability of Atg9p to recycle from the PAS to a peripheral pool is an important aspect of Atg9p function in autophagy in yeast.

As a first step towards understanding the function of Atg9 in mammalian cells, we have identified and characterized mammalian Atg9 (mAtg9) under both normal growth conditions and starvation. We show that mAtg9 is a polytopic multi-spanning membrane protein, with both termini in the cytoplasm. Endogenous mAtg9 is found both on juxta-nuclear TGN membranes and late endosomes. After starvation, the juxta-nuclear TGN46 colocalized pool of mAtg9 is diminished, leaving a dispersed peripheral pool. This pool of mAtg9 colocalizes with Rab7 and the AV marker GFP-LC3. The change in distribution of mAtg9 after starvation is inhibited by small interference RNA (siRNA)-mediated depletion of ULK1 (the putative mammalian orthologue of Atg1), resulting in retention of the juxta-nuclear pool of mAtg9. Treatment with inhibitors of phosphatidylinositol 3-kinase (PI 3-kinase) also blocked the starvation-induced redistribution of mAtg9. Finally, upon re-addition of amino acids, mAtg9 recycled back to the juxta-nuclear region. Interestingly, under all the conditions we studied, the cation independent mannose-6-phosphate receptor (CI-MPR) distribution was affected in a similar way to mAtg9. Our results suggest that in mammalian cells mAtg9 traffics to and from the TGN and late endosomes. We speculate that either the ability of mAtg9 to undergo this trafficking step or the actual machinery involved in trafficking to and from the TGN to endosomes plays a role in starvation-induced autophagy.

Results

Identification of mAtg9

Using bioinformatics we identified a putative human homologue of yeast Atg9p (supplementary material Fig. S1A), that is identical to the recently described APG9L1 (Yamada et al., 2005). Following the agreed nomenclature for genes involved in autophagy (Klionsky et al., 2003), we refer to APG9L1 and the rat homologue as mAtg9. Northern blot analysis shows that the human Atg9 mRNA is enriched in skeletal muscle, heart and placenta (supplementary material Fig. S1B), consistent with the distribution of APG9L1 (Yamada et al., 2005). Alignment of the mAtg9 sequence with homologues from other organisms revealed that the central region of the protein, containing between three and five predicted transmembrane domains (TMDs), is highly conserved (supplementary material Fig. S2). Outside this region, the position of two additional predicted N-terminal TMDs is also well conserved. Finally, there are four potential sites for N-linked glycosylation (see Fig. 1A, supplementary material Fig. S1A).

Characterization of mAtg9 in HEK293 cells

Antibodies specifically recognizing the N- or C-termini of both human and rat mAtg9 (Fig. 1A) were used to characterize the subcellular localization of endogenous mAtg9 in HEK293 cells (Fig. 1B). Although both epitopes are conserved in rat and human they are not found in the homologous protein APG9L2 (Robb et al., 2004). Both the N- and C-terminal specific antibodies recognise a 105 kDa protein in HEK293 cell lysates, which is lost upon targeted siRNA knockdown (supplementary material Fig. S3). Both antibodies labelled juxta-nuclear and peripheral structures (Fig. 1B), although the relative intensity of the mAtg9 signal in the two populations varied between cell lines. An HA-tagged mAtg9 displayed a similar localization in cells expressing low levels of the transfected protein (Fig. 1C). siRNA-mediated depletion of endogenous mAtg9 reduced both the peripheral and juxta-nuclear pools to below detection levels (supplementary material Fig. S3).

Topology of mAtg9

Topology prediction algorithms identify 5 to 7 TMDs within mAtg9, whilst a cross species analysis shows that 6 of the putative TMDs are highly conserved (supplementary material Fig. S2). To define the topology of mAtg9, we first exploited the presence of 4 potential sites for N-linked glycosylation within the polypeptide. Two of these sites are between TMD1 and TMD2, the next between the TMD2 and TMD3, while the fourth is in the C-terminal domain (see Fig. 1A). We treated lysates from HEK293 cells with glycosidases PNGaseF and EndoH and found that endogenous mAtg9 contains complex N-glycans (Fig. 1D). To identify the glycosylation sites used, we systematically mutated the candidate residues N99, N224, and N507 to D (note, N129 is too close to a TMD to be a likely candidate for N-glycosylation), and expressed HA-tagged wild-type and mutant proteins in HEK293 cells (Fig. 1E). Like the endogenous protein, the HA-tagged wild-type protein was sensitive to PNGaseF (Fig. 1E, lanes 1 and 2). Mutation of N99 abolished the glycosylation and only the ~80kDa non-glycosylated form was seen (Fig. 1E, lanes 3 and 4). Mutation of N224 and N507 resulted in a wild-type behaviour (Fig. 1E, lanes 5 and 6). The triple mutant was not glycosylated (Fig. 1E, lanes 7 and 8). Since N99 is N-glycosylated, we conclude that the first loop of mAtg9 is translocated into the lumen of the ER, suggesting that the N-terminus of the protein is in the cytosol.

To confirm this and to investigate the topology of the other TMDs, we performed in vitro synthesis experiments. We used an N-terminal 183 aa fragment of the wild-type and N99D mAtg9 because these contained the only utilized N-linked glycosylation site, and the shorter fragment facilitated the analysis of the topology of the N-terminus. When these fragments were synthesized in the presence of [^{35}S]-methionine and ER microsomes, the wild-type fragment generated two products, the larger of which was sensitive to Endo H and, hence, N-glycosylated (Fig. 1F, lanes 1 and 2). The N99D mutant was not glycosylated (Fig. 1F, lanes 3 and 4). Likewise, in vitro analysis of the full-length proteins showed that all of the mutants, except N99, resembled the wild-type (wt) protein (data not shown). We conclude that only N99 is glycosylated both in vitro and in vivo.

To determine whether the N- and C-termini of mAtg9 are lumenal or cytosolic, protease protection experiments were performed with both the N-terminal fragment (Fig. 1G) and the full-length protein (Fig. 1H). Proteinase K treatment of ER microsomes without or with Triton X-100 after in vitro synthesis of the 183 aa truncation fragment, followed by

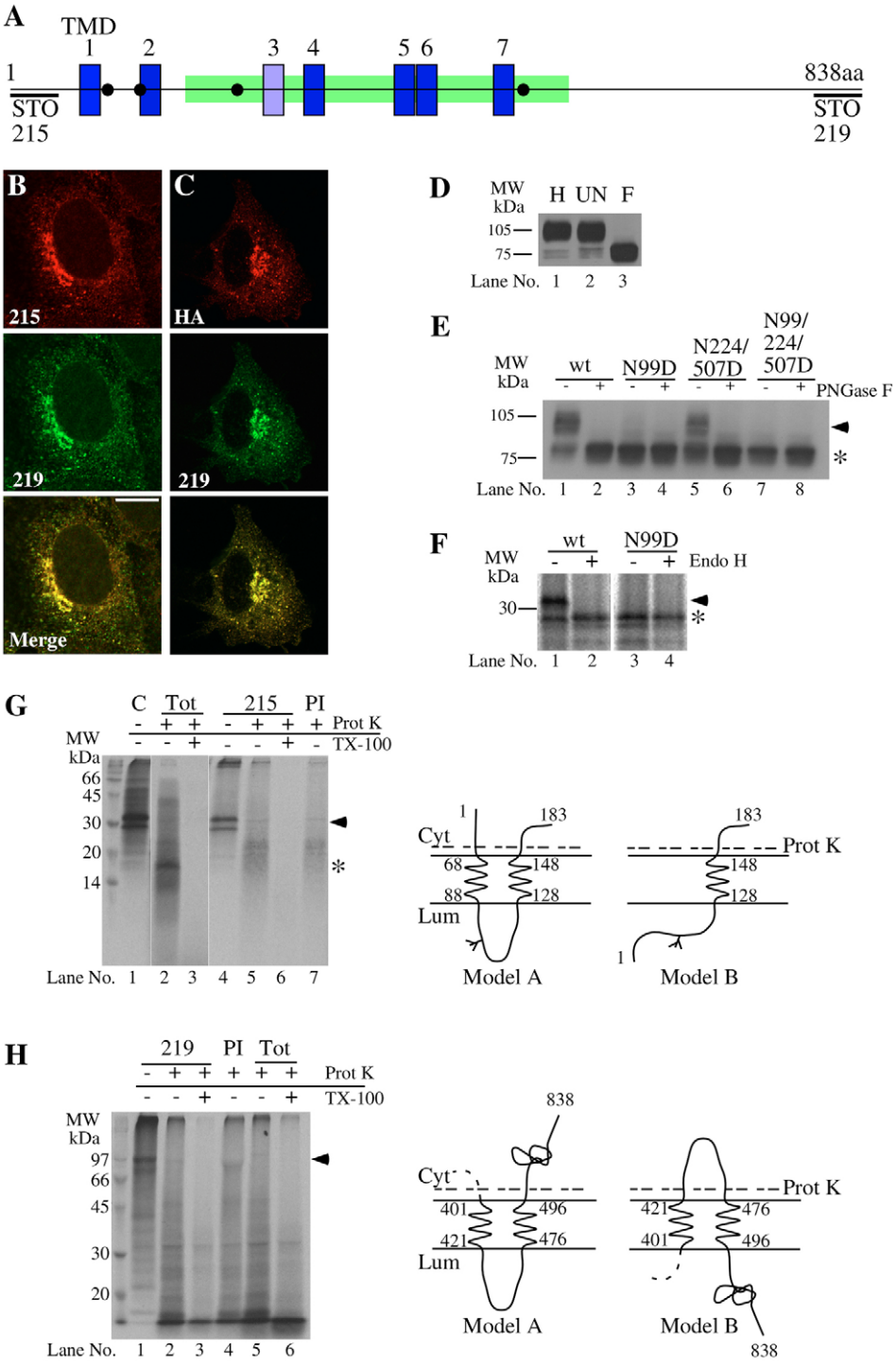

Fig. 1. Distribution and topology of mAtg9. (A) Proposed topology of mAtg9 shown with seven transmembrane domains (TMDs). The conserved Atg9 PFAM domain is shown in green. Black dots represent potential N-glycosylation sites. Antibodies raised against the N- and C-termini were designated STO215 and STO219, respectively. (B) Immunofluorescence in HEK293 cells with Alexa Fluor-488- and Alexa Fluor-555-conjugated mAtg9 antibodies. (C) Indirect immunofluorescence of HA-tagged mAtg9 and anti-Atg9 (STO219). Bar, 10 μm. (D) HEK293 PNS was treated with glycosidases, EndoH (lane 1) or PNGaseF (lane 3). UN, untreated (lane 2). PNGaseF treatment altered the migration of mAtg9 from 105 kDa to 75 kDa. (E) Lysates from HEK293 cells transiently transfected with wt HA-mAtg9 (lanes 1 and 2), HA-mAtg9 N99D (lanes 3 and 4), N224/507D (lanes 5 and 6) or N99/224/507D (lanes 7 and 8) were treated (+) or not (–) with PNGaseF. The N99D and N99/224/507D mutants were not glycosylated (lower band, *), whereas the N224/507D mutant was glycosylated (upper band, arrowhead) and sensitive to PNGaseF. (F) An in vitro synthesized 183 aa N-terminal mAtg9 fragment was treated (+) or not (–) with EndoH. The wt sequence fragment (lanes 1 and 2) was glycosylated (upper band, arrowhead), and sensitive to EndoH, whereas the N99D mutant fragment (lanes 3 and 4) was not (lower band, *). (G) Topology of the N-terminus: ER microsomes, containing the 32 kDa, 183 aa fragment (lane 1), were treated with proteinase K (Prot K) in the absence of TX-100 (lane 2) resulting in two bands migrating at ~14 kDa and ~18 kDa (*), which correspond to the protected glycosylated and non-glycosylated forms of the TM1, TM2 and their inter-TMD loop (see Model A). No bands were detected after Prot K treatment in the presence of Triton X-100 (TX-100, lane 3). The 183 aa fragment could be immunoprecipitated using anti-N-terminal STO215 (lane 4), but not after Prot K treatment in the absence (lane 5) or presence (lane 6) of detergent, consistent with the removal of the N-terminal epitope (Model A). Note: If the N-terminus were lumenal (see Model B), then a ~25 kDa band would have been detected. The numbers shown on the models refer to amino acid position. C, control, PI, pre-immune serum, Tot, totals, i.e. non-IPs, Cyt, cytosol, Lum, lumen. (H) Topology of C-terminus. Full-length in-vitro-synthesized mAtg9 was immunoprecipitated using anti-C-terminal STO219 (lane 1, arrowhead). After Prot K treatment of the microsomes in the absence of TX-100 no fragment was immunoprecipitated (lane 2), consistent with removal of the C-terminal epitope (Model A). Note: If the C-terminus were lumenal, then a ~40 kDa fragment would have been expected (Model B). Controls are as for panel G.

immunoprecipitation using the N-terminal anti-Atg9 (215) antibody, resulted in no detectable bands at ~30 kDa (Fig. 1G, lanes 5 and 6) compared with controls (Fig. 1G, lane 1 and 4). Thus, the N-terminus of mAtg9 was degraded upon protease digestion of the membrane-integrated N-terminal fragment (Fig. 1, Model A). This result confirms that TMD1 is a bona fide TMD and that the N-terminus of the protein is cytosolic. Likewise, whereas full-length mAtg9 synthesized in a cell-free

system was immunoprecipitated by the C-terminal-specific anti-Atg9 (219) antibody (Fig. 1H, lane 1), no membrane-dependent fragment was found to be protease protected and specifically recognised by this antibody (Fig. 1H, lanes 2-3). An ~40 kDa C-terminal fragment should be protected from proteinase K digestion without detergent if the C-terminus was in the ER lumen, but only limited digestion products were detected (Fig. 1H, lane 2). We therefore conclude that the C-terminus of mAtg9 is cytosolic (Fig. 1H, Model A).

A live-cell imaging assay was used to confirm the orientation of the N-terminus of mAtg9 in vivo (Lorenz et al., 2006). NRK cells were co-transfected with an ER transmembrane protein containing a lumenal YFP and cytosolic CFP tag, and monomeric RFP (mRFP) tagged to the N-terminus of mAtg9. Both the YFP and CFP fluorescent signals can be detected in the ER (Fig. 2A). mRFP-mAtg9 shows a peri-nuclear localization but can also be detected in the ER, consistent with some of the N-terminally tagged mAtg9 protein being retained in the ER at higher expression levels. When transfected cells were treated with digitonin under conditions which permeabilize the plasma membrane and leave other intracellular membranes intact, all three fluorescent signals were detected (Fig. 2B). Subsequent trypsin digestion of the protein domains on the cytosolic face of the membranes reduced the fluorescence of both the cytosolic CFP-ER marker and the N-terminal mRFP tag on mAtg9, but not the YFP tag (Fig. 2C). A C-terminal mRFP fusion with mAtg9 was distributed abnormally compared with the endogenous protein and was not further analysed. The ER accumulation and abnormal distribution of the overexpressed N- and C-terminal tagged mAtg9 in these and other cell lines precluded a detailed analysis of the trafficking of tagged mAtg9 by cell imaging techniques. Nonetheless, this experiment provides a direct demonstration that in vivo the N-terminus of mAtg9 is located in the cytosol, in agreement with both the glycosidase and in vitro synthesis experiments. Our data, taken together with the topology prediction algorithms predictions, support a model where mAtg9 spans the membrane six times, with both N- and C-termini located in the cytosol. We predict that TMD 1 and 2 and TMDs 4-7 (see Fig. 1, supplementary material Fig. S2B) are genuine TMDs and that the putative TMD3 is not in the membrane.

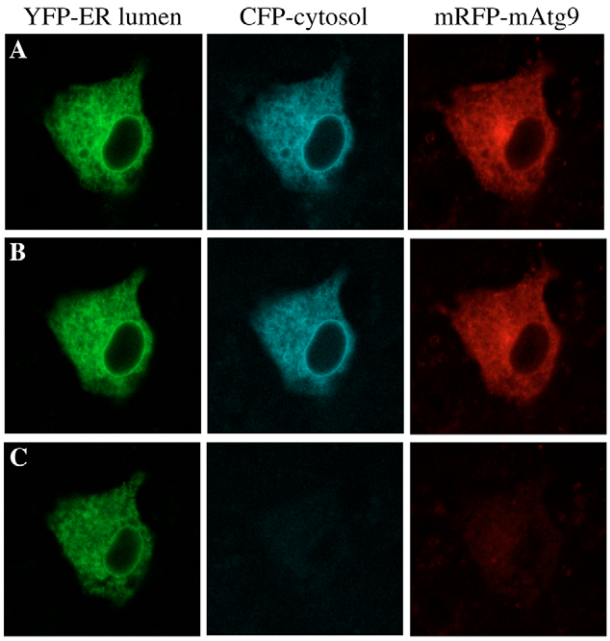

Fig. 2. In vivo topology analysis of mAtg9. Plasmids YFP-HLA-A2-CFP and mRFPmAtg9 were transiently transfected into NRK cells. YFP on the N-terminus is in the ER lumen and CFP on its C-terminus is cytosolic. (A) Pre-treatment images. (B) Images captured after 2 minutes of permeabilization with digitonin. (C) Images captured 5 minutes after subsequent trypsin addition. At the concentration used, digitonin permeabilized the plasma membrane but not the ER. Lumenal YFP on the N-terminus of HLA-A2 was protected from the trypsin, but the C-terminal CFP and the mRFP on the N-terminus of mAtg9 were degraded by the trypsin and are therefore cytosolic. All images were captured using identical imaging parameters.

mAtg9 localizes to the trans-Golgi network

To clarify the subcellular localization of mAtg9, we compared the endogenous mAtg9 distribution to the ER-specific marker protein disulfide isomerase (PDI), the ER-Golgi-intermediate compartment (p58) and the Golgi complex (Fig. 3). As shown in Fig. 1, the endogenous protein has complex EndoH-resistant glycans indicating transit through the medial and trans-Golgi complex. Whereas PDI showed little colocalization with mAtg9, there was partial colocalization with p58 (data not shown). In addition, mAtg9 showed greatest colocalization with the trans-Golgi network marker TGN46 (Fig. 3C), although partial colocalization with the medial Golgi marker GM130 was detected (Fig. 3A). Nocodazole perturbation of the Golgi complex results in the formation of mini-stacks, altering the distribution of both GM130 and TGN46 (Turner and Tartakoff, 1989). After nocodazole treatment, GM130, TGN46 and mAtg9 dispersed throughout the cell (Fig. 3B,D), and mAtg9 showed better colocalization with TGN46 than with GM130 in the dispersed mini-stacks (Fig. 3, compare insets in D with B). Localization of mAtg9 to the Golgi was confirmed by immunogold labelling in HEK293 cells with anti-GM130 and mAtg9 antibodies (Fig. 3E). Whereas GM130 labelled the Golgi cisternae, mAtg9 was found on the edges of the Golgi cisternae and, occasionally, on vesicles close to the Golgi complex, which – based on its colocalization with TGN46 – might represent TGN membranes. Additional support for localization of mAtg9 on TGN membranes was obtained using subcellular fractionation to purify a stacked Golgi fraction from rat liver (Slusarewicz et al., 1994). Importantly, TGN membranes are largely separated from Golgi membranes by this procedure, being only present at 10-15% of their original level (Nakamura et al., 1995). Using this strategy, we found mAtg9 partitions with TGN38, but not mannosidase II (a marker for cis- and medial-Golgi) or p58 (supplementary material Fig. S4).

mAtg9 is present in late endosomes

Having shown that the juxta-nuclear pool of mAtg9 overlaps with TGN membranes, we addressed the identity of the peripheral mAtg9 pool. We reasoned that the compartment might be endosomal because many TGN proteins, including the CI-MPR, cycle between the TGN and endosomes.

We fractionated early and late endosomes from rat liver

(Ellis et al., 1992) and compared the distribution of mAtg9 and other markers across the gradient (Fig. 4A). We used horseradish peroxidase (HRP)-conjugated biotin – internalized for 10 minutes and chased for 20 minutes – to identify late endosomes, which are found in fractions 22-25. Early endosomes identified by EEA1 are found in fractions 23-27. CI-MPR is found in fractions that partially overlap with HRP-biotin as well as in denser fractions. mAtg9 co-fractionates with the internalized HRP-biotin but it is also found in heavier fractions containing CI-MPR and TGN38-positive membranes (Fig. 4A).

To further characterize the peripheral pool of mAtg9, we compared the distribution of mAtg9 with markers for early and late endosomes by indirect immunofluorescence in HEK293 cells. We confirmed the colocalization of mAtg9 with CI-MPR in a juxta-nuclear and peripheral region (Fig. 4B), and the lack of colocalization with markers for early endosomes or lysosomes (EEA1 and LAMP2, respectively; data not shown). Cryo-immunogold labelling of HEK293 cells additionally demonstrated the presence of mAtg9 on late endosomes, identified by the presence of internalized 6-nm bovine serum albumin (BSA)-conjugated-gold and the CI-MPR (Fig. 4C).

We next asked whether mAtg9 colocalized with the small-GTPase proteins Rab4, Rab5, Rab6, Rab7, Rab9 and Rab11. GFP-fusions of the early endosomal Rab proteins, GFP-Rab4, GFP-Rab5 and GFP-Rab11 (Sonnichsen et al., 2000), showed no colocalization with mAtg9 (data not shown). As expected, GFP-Rab6, localized to the peri-nuclear TGN region (Goud et al., 1990), showed good colocalization with mAtg9 (Fig. 5A). Both GFP-Rab7 and GFP-Rab9, which localize to distinct populations of late endosomes (Barbero et al., 2002), showed an overlap with mAtg9 (Fig. 5B,D). In addition, we found good colocalization between endogenous Rab7 and Rab9, and mAtg9 (Fig. 5C,E). Note, endogenous Rab7 was detected after pre-permeabilization with low concentrations of saponin. The colocalization of Rab7, Rab9, and CI-MPR with mAtg9 suggests that a population of mAtg9 is present on late endosomes. Thus, our data indicate that mAtg9 is present in two locations, the TGN and late endosomes, and we suggest mAtg9 cycles between these compartments.

mAtg9 colocalizes with GFP-LC3 and Rab7 after starvation

Although it has been demonstrated that siRNA depletion of Atg9L1 inhibits the appearance of GFP-LC3-positive dots during a 24-hour starvation period (Yamada et al., 2005), it is not known how the localization of the endogenous mAtg9 is affected by starvation, or whether mAtg9 localizes to AVs. In yeast, Atg9 was not found on AVs accumulated in the vacuole in Pep4-deficient strains (Lang et al., 2000; Noda et al., 2000). We starved HEK293 cells stably expressing GFP-LC3 (Köchl et al., 2006) for 2 hours in Earle's saline (ES) to stimulate the formation of AVs, and looked at colocalization of endogenous mAtg9 and GFP-LC3 (Fig. 6A). During starvation there was a significant loss of the juxta-nuclear mAtg9 signal, an increased colocalization with Rab7, as well as the appearance of mAtg9, GFP-LC3-positive structures (Fig. 6A). Quantification revealed that 45% of the GFP-LC3-positive structures contained mAtg9 (Table 1), although the amount of mAtg9 localized with GFP-LC3-positive structures was low (7%). The colocalization of endogenous mAtg9 with GFP-LC3 is

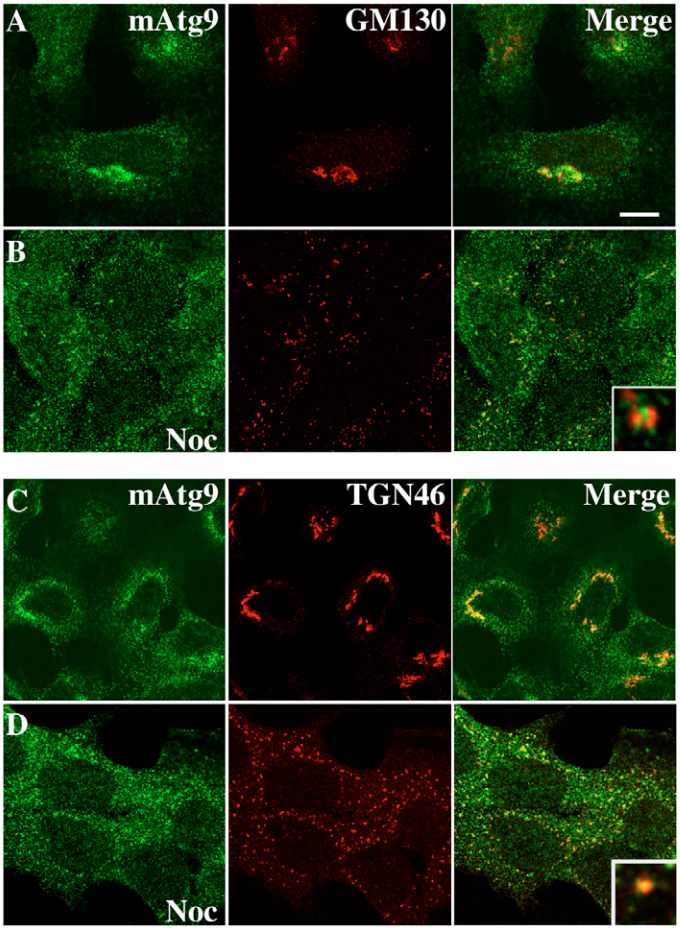

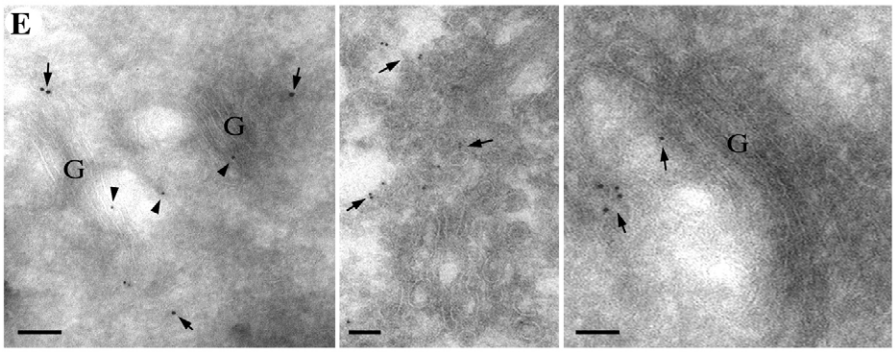

Fig. 3. mAtg9 localizes to the trans-Golgi network. HEK293 cells were labelled with antibodies to mAtg9 and GM130 (A,B) or TGN46 (C,D). Cells in B and D were treated for 30 minutes with nocodazole (noc). Insets illustrate the colocalization after noc treatment. Bar, 10 μm. (E) Immunogold labelling of mAtg9 (10-nm gold, arrows) and GM130 (5-nm gold, arrowheads (left panel) in HEK293 cells. G, Golgi. Bars, 200 nm.

consistent with recent data, showing that overexpressed mAPG9L1-DsRed2 colocalized with GFP-LC3 after 24 hours of starvation (Yamada et al., 2005).

AVis are not Rab7-positive and do not contain degradative enzymes, whereas AVds have acquired both Rab7 and degradative enzymes (Gutierrez et al., 2004; Jager et al., 2004). We found that, after 2 hours starvation approximately 50% of the GFP-LC3-positive AVs were also positive for Rab7, indicating that about half of the GFP-LC3-positive structures are AVds. However, of the structures that were double positive for mAtg9 and Rab7 (30%) only 7% at most contain GFP-LC3 (Table 1).

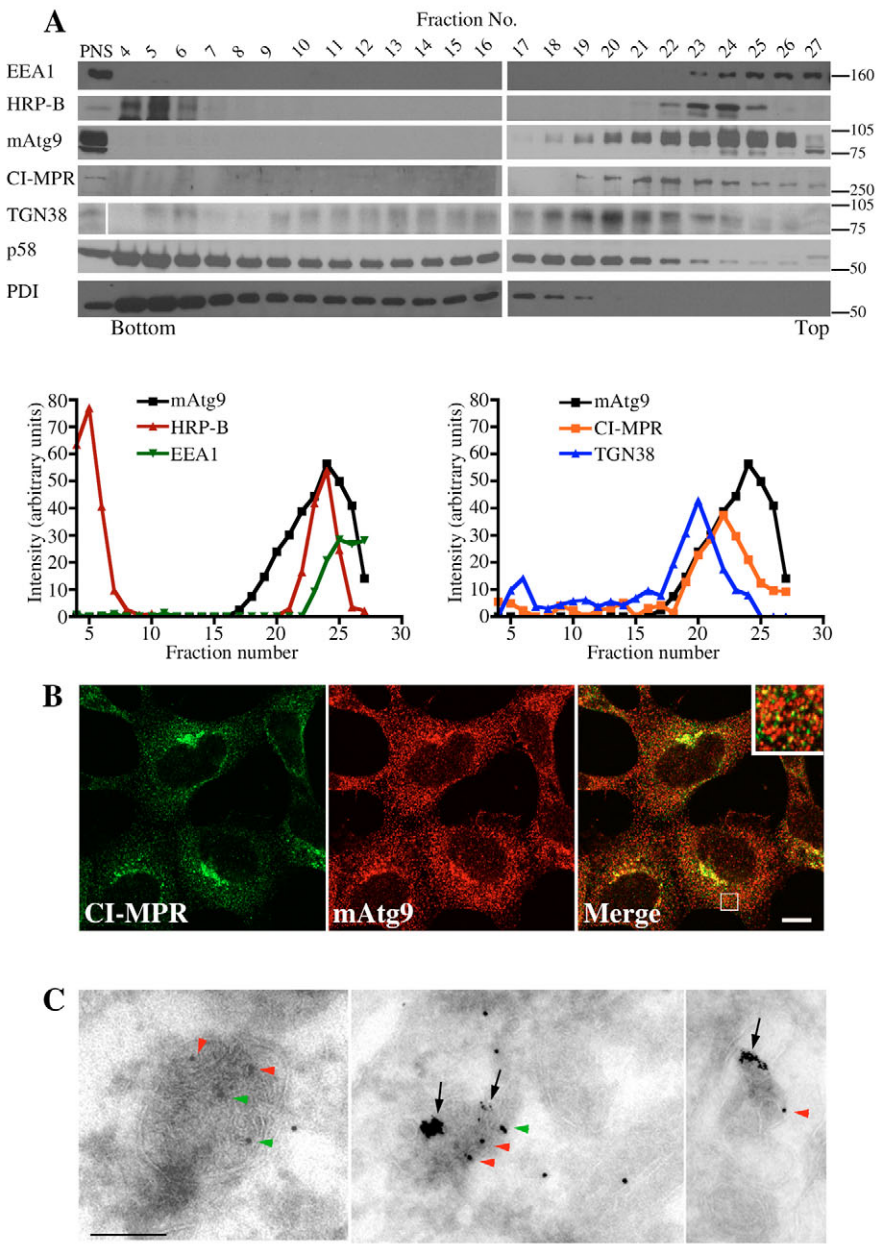

Fig. 4. mAtg9 is present on late endosomes. (A) Western blots of fractions from an endosome preparation gradient from rat liver using antibodies for EEA1 (early endosomes), mAtg9, CI-MPR, TGN38 (TGN), p58 and PDI (ER). To label late endosomes, HRP-biotin was internalized by perfusion for 10 minutes followed by a 20-minute chase before homogenization. HRP-biotin was detected using ExtraAvidin-HRP. Signals were quantified by densitometry, performed using ImageJ. Data are representative of two independent experiments. (B) mAtg9 colocalizes with the CI-MPR in indirect immunofluorescence on HEK293 cells. Inset is enlargement of the peripheral staining in the merge. Bar, 10 μm. (C) Cryoimmunogold labelling of mAtg9 (red arrowheads, 10-nm gold), CI-MPR (green arrowheads, 15-nm gold), on HEK293 cells labelled with 6-nm conjugated BSA-Gold (arrows) internalized for 2 hours. Bar, 200 nm.

mAtg9 knockdown by siRNA, which resulted in a greater than 90% loss of mAtg9 (supplementary material Fig. S3), resulted in a modest decrease in the conversion of GFP-LC3-I by lipidation to GFP-LC3-II during starvation – a robust read-out for autophagy (Mizushima, 2004) (Fig. 6B) – and a statistically significant decrease in long-lived protein degradation (Fig. 6C). However, loss of mAtg9 to levels below detection did not result in a complete absence of GFP-LC3-positive puncta after 2 hours of starvation (data not shown). Thus, from our quantitative colocalization analysis, our data on the inhibition of protein degradation after siRNA depletion and previously published data (Yamada et al., 2005), we conclude that mAtg9 is found on both GFP-LC3-positive AVis and AVds, and is required for autophagy.

mAtg9 trafficking is altered during starvation

In *S. cerevisiae*, after nitrogen starvation, Atg9p cycles to the PAS from a dispersed peripheral pool (Kim et al., 2002; Noda et al., 2000) that has been recently suggested to be mitochondrial (Reggiori et al., 2005). Since we have demonstrated Golgi and also endosomal pools of mAtg9, we hypothesized that mAtg9 cycles between TGN and endosomes, and that this recycling could be affected by starvation. Indirect immunofluorescent labelling of mAtg9 in HEK293 cells incubated in ES medium (Fig. 7B) confirmed that the juxta-nuclear mAtg9 signal largely disappeared compared with unstarved cells (Fig. 7A) and the peripheral signal remained.

After starvation, we noted that the extent of colocalization of mAtg9 with CI-MPR (Fig. 7B) did not decrease in a similar way as compared with TGN46 (Fig. 7E). Rather, the distribution of CI-MPR also appeared to be slightly affected by the incubation in ES medium. An alternative method of inducing autophagy is by treatment with rapamycin which inhibits TOR (target of rapamycin), a negative regulator of autophagy (Noda and Ohsumi, 1998). Treatment of HEK293 cells with rapamycin for 2 hours

in full medium (FM) caused the redistribution of mAtg9 away from the juxta-nuclear region (Fig. 7C). The distribution of CI-MPR but not TGN46, was also affected by rapamycin (Fig. 7C and data not shown). In both, ES and FM supplemented with rapamycin, the extent of colocalization of mAtg9 and CI-MPR was similar to the unstarved controls.

Autophagy is inhibited by PI 3-kinase inhibitors (Blommaart et al., 1997). Therefore, we treated cells during starvation with LY290042, and asked whether the starvation-induced redistribution of mAtg9 was inhibited. As shown in Fig. 7D,F, mAtg9 dispersion was inhibited resulting in an increased colocalization with TGN46, whereas there was no change in the colocalization with CI-MPR. Both mAtg9 and CI-MPR in cells kept in ES medium with LY294002 (Fig. 7D) resembled that seen in cells kept in FM (Fig. 7A). Treatment of unstarved HEK293 cells with LY290042 had no effect on the steady-state localization of mAtg9 or CI-MPR (data not shown).

Lastly, because we hypothesized that the peripheral population of mAtg9 was derived from the juxta-nuclear pool, we tested whether re-addition of amino acids after starvation and in the presence of cycloheximide, could recover the juxta-nuclear pool of mAtg9. Two hours after re-addition of FM (Fig. 7G), we found an increased colocalization of mAtg9 with TGN46 compared with starvation (Fig. 7E). These data support our hypothesis that the mAtg9 is cycling between the juxta-nuclear TGN region, and a peripheral endosomal region, and this cycling is perturbed by starvation and rapamycin treatment in a PtdIns 3-kinase sensitive manner.

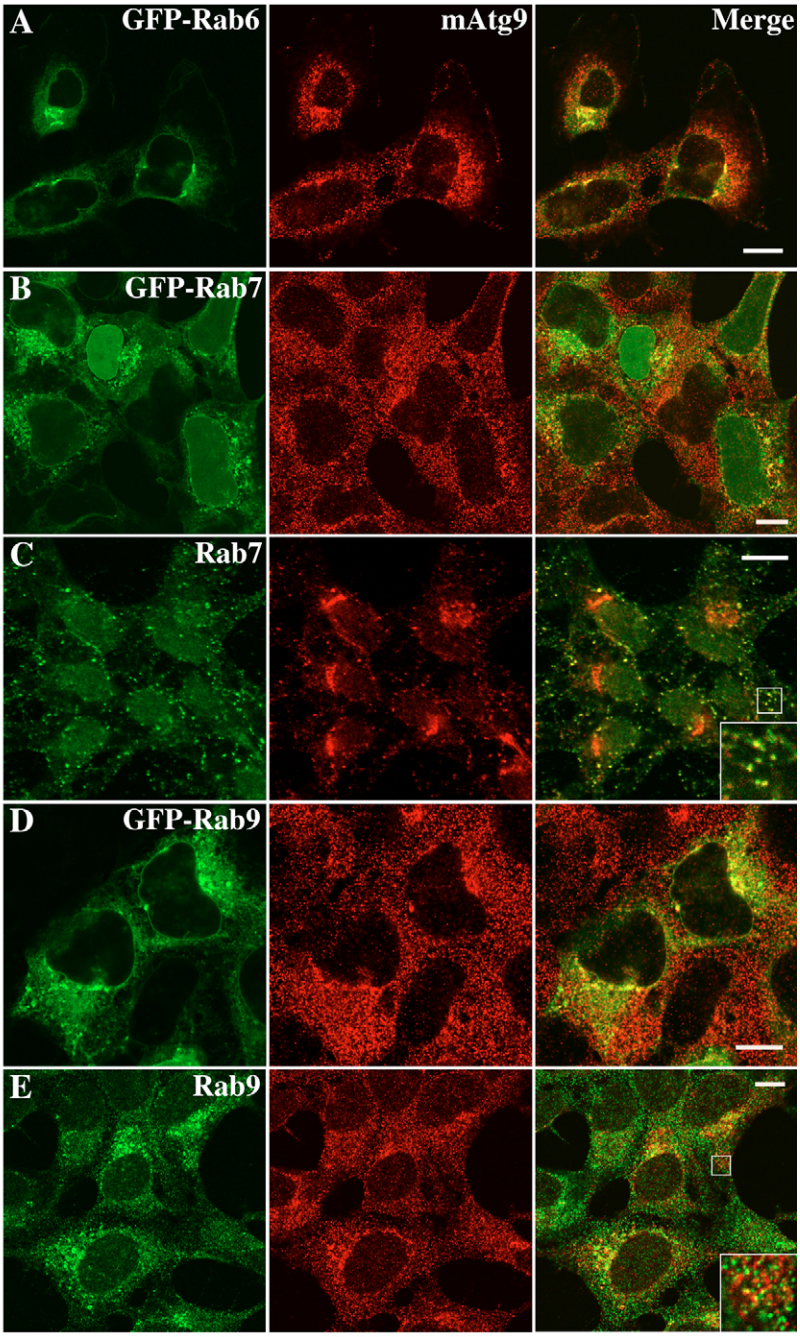

Fig. 5. mAtg9 colocalizes with Rab6 on Golgi membranes, and Rab7 and 9 on late endosomes. HEK293 cells were transiently transfected with GFP-Rab6 (A), GFP-Rab7 (B) and GFP-Rab9 (D), then 24 hours later fixed and labelled with the mAtg9 antibody. Cells were also labelled with antibodies to endogenous Rab7 (C) and 9 (E), the inset is an enlargement of the merge to show the peripheral staining. For Rab7 staining, cells were extracted using 0.05% (w/v) saponin before fixation. Bars, 10 μm.

mAtg9 trafficking is dependent on mAtg1 (ULK1)

To elucidate whether the starvation-dependent redistribution of mAtg9 reflected an autophagy-specific signal, we employed a knockdown screen of several mammalian *ATG* genes and asked whether mAtg9 redistribution could be inhibited. Since *S. cerevisiae* Atg9p (ScAtg9p) retrieval from the PAS depends on ScAtg1p (Reggiori et al., 2004) it seemed likely that knockdown of the putative mammalian Atg1 homologue might affect mAtg9 cycling. HEK293 cells were treated with siRNA duplexes specific for human ULK1 (mAtg1), mAtg5, Beclin1 (mAtg6), mAtg7, mAtg12. After 72 hours, siRNA-mediated depletion of mAtg5 and Beclin1 was confirmed by western blot (data not shown). Depletion of ULK1 and mAtg7 was confirmed by a reduction in GFP-LC3-II and reverse transcriptase (RT)-PCR (supplementary material Fig. S5 and data not shown).

In starved HEK293 cells, depletion of ULK1 inhibited the redistribution of mAtg9 from the TGN46-positive juxta-nuclear region to the peripheral pool, resulting in a distribution comparable with unstarved controls (Fig. 8C). Importantly, there was no discernible change in TGN46 distribution after ULK1 knockdown and starvation. ULK1 belongs to a family of relatively uncharacterized serine/threonine kinases including ULK2, the next closest member of this family to ScATG1. The specificity of ULK1 activity on mAtg9 was

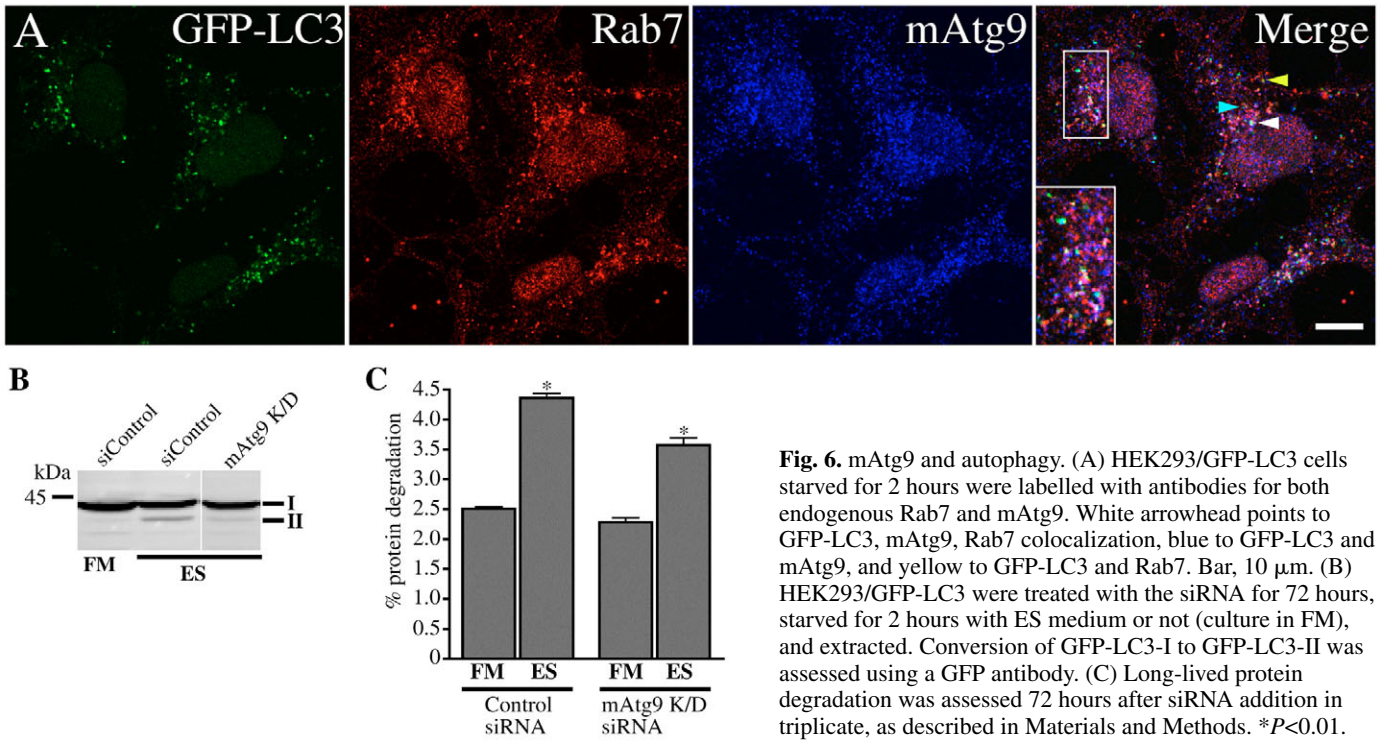

Fig. 6. mAtg9 and autophagy. (A) HEK293/GFP-LC3 cells starved for 2 hours were labelled with antibodies for both endogenous Rab7 and mAtg9. White arrowhead points to GFP-LC3, mAtg9, Rab7 colocalization, blue to GFP-LC3 and mAtg9, and yellow to GFP-LC3 and Rab7. Bar, 10 μm. (B) HEK293/GFP-LC3 were treated with the siRNA for 72 hours, starved for 2 hours with ES medium or not (culture in FM), and extracted. Conversion of GFP-LC3-I to GFP-LC3-II was assessed using a GFP antibody. (C) Long-lived protein degradation was assessed 72 hours after siRNA addition in triplicate, as described in Materials and Methods. *P<0.01.

Table 1. Quantification of GFP-LC3, Rab7 and mAtg9 co-localization

GFP-LC3 with Rab7	Rab7 with GFP-LC3	GFP-LC3 with mAtg9	mAtg9 with GFP-LC3	Rab7 with mAtg9	mAtg9 with Rab7
51.2±9.4%	6.7±1.2%	45.9±0.6%	7.4±0.7%	26.8±3.7%	32.3±5.0%

Images were analysed using the co-localization function of the Zeiss LSM-510 software. Quantification was performed for each cell, using a region of interest, and data are the mean values of 20 cells obtained from two independent experiments, %±s.e.m.

examined by knocking down ULK2 (Fig. 8D). ULK2 knockdown, confirmed by RT-PCR (data not shown), had no effect on the localization of mAtg9. In addition, ULK2 knockdown, or knockdown of other ULK family members, had no effect on induction of autophagy (E.C. and S.T., unpublished data).

siRNA-mediated depletion of the other Atg proteins did not show a dramatic effect on mAtg9. We quantified the effects of the various knockdowns after starvation using colocalization of mAtg9 with TGN46. As shown in Table 2, approximately 50% of mAtg9 in the juxta-nuclear region colocalized with TGN46 in FM, decreasing to 30% after starvation. ULK1 knockdown under starvation conditions increased the colocalization of mAtg9 with TGN46 to 60%. ULK2, Atg5, Atg7 and Atg12 did not significantly increase the colocalization of mAtg9 with TGN46 after starvation. Although Beclin1 knockdown resulted in a slight increase in the juxta-nuclear colocalization of mAtg9 and TGN46, from 30% to 42%, it did not reach the level of colocalization seen in FM, and was difficult to detect by visual inspection of the cells by confocal microscopy. The degree of colocalization of mAtg9 and CI-MPR remained constant (Fig. 8E-G), adding further support to the data that the mAtg9 and CI-MPR were affected similarly by starvation and ULK1 knockdown.

Discussion

Localization and topology of mAtg9

We have found that mAtg9 is present on both the TGN and late endosomes, colocalizing with TGN46, CI-MPR, Rab9 and Rab7. The presence of mAtg9 in these two locations suggests that at steady-state, the protein is cycling between these two compartments, and that the localization of mAtg9 is different from ScAtg9, and *P. pastoris* Atg9 (PpAtg9), where Atg9 was not found on ER, Golgi or endosomes but in a peri-vacuolar region, the PAS, and peripheral membranes (Chang et al., 2005; Lang et al., 2000; Noda et al., 2000). Recently, Reggiori

Table 2. Percentage co-localization of mAtg9 with TGN46 upon starvation after knocking down Atg proteins

Culture medium	FM	ES						
RNAi	siC	siC	ULK1	ULK2	Beclin	Atg5	Atg7	Atg12
Average±s.e.m.	51.2±1.2%	29.1±1.7%	61.6±1.9%	32.9±2.6%	41.6±1.6%	31.9±1.9%	32.7±1.5%	34.4±2.2%

Images were analysed using the co-localization function of the Zeiss LSM-510 software. Quantification was performed using a region of interest surrounding the TGN staining and data are the mean values of 10 cells from a representative experiment.

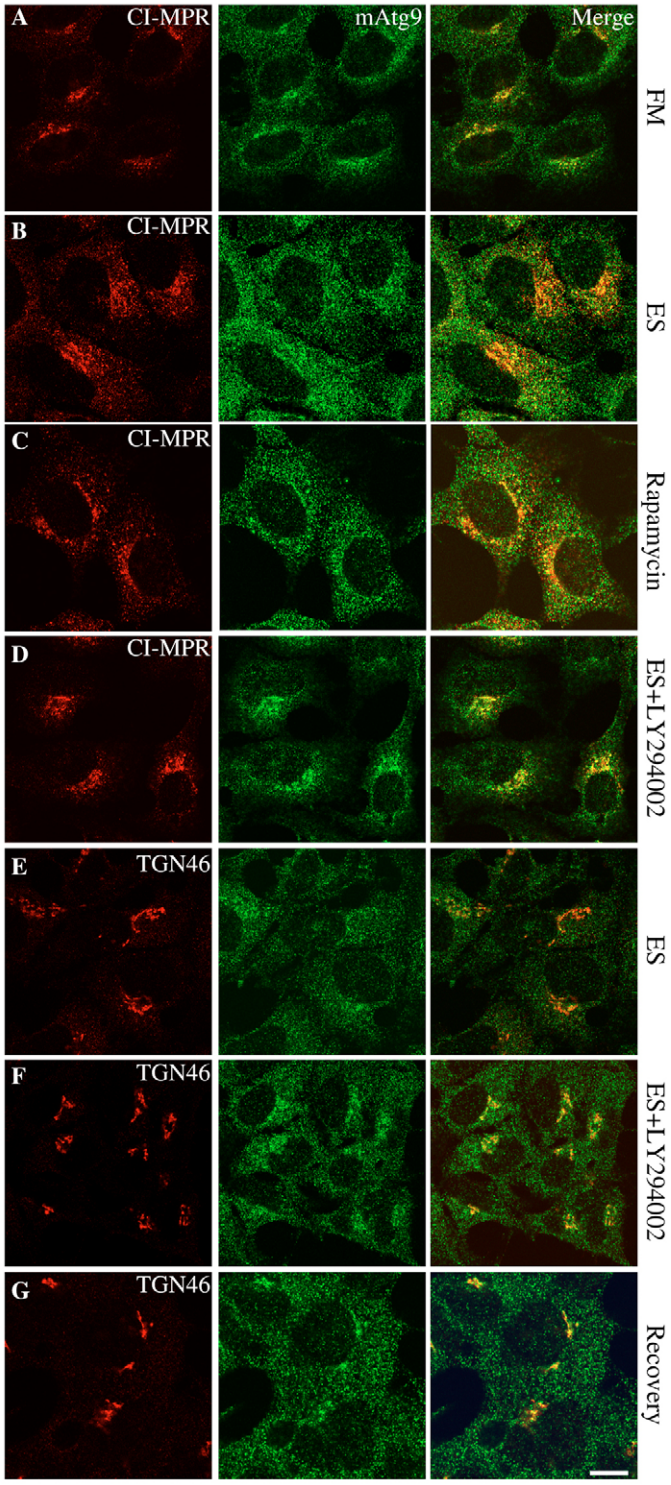

Fig. 7. mAtg9 and CI-MPR redistribute upon starvation in a reversible, PtdIns 3-kinase-dependent manner. HEK293 cells were labelled with antibodies against mAtg9 and CI-MPR (A-D) or TGN46 (E-G). Cells had first been treated with either rapamycin (C) for 2 hours, or for 2 hours in ES medium in the presence (D,F) or absence (B,E) of 65 μM LY294002. (G) Cells had been starved for 2 hours in ES medium, before incubation in FM for 2 hours in the presence of 10 μg/ml cyclohexamide. Note: cyclohexamide was also included in the final 15 minutes in ES medium). Bar, 10 μm.

et al. demonstrated that some of the ScAtg9-positive peripheral structures are associated with mitochondria, despite the lack of a mitochondrial targeting sequence (Reggiori et al., 2005). We found no evidence that endogenous or overexpressed mAtg9 was present on mitochondria, in agreement with recent data concerning overexpressed APG9L1 and APG9L2 (Yamada et al., 2005). However, it cannot be excluded in our cell system that this association is transient and difficult to detect at steady-state or that it is unstable after lysis of cells.

Our data on mAtg9 topology demonstrate that the N- and C-termini of mAtg9 are localized in the cytosol, and support topology predictions of TopPred II and MemStat that the protein spans the membrane six times. This topology is further corroborated by our finding that mAtg9 contains one N-linked glycan at N99 in the loop between TMD1 and TMD2. Interestingly, several well-characterized motifs (tyrosine and di-leucine motifs) (Bonifacino and Traub, 2003) are present within the cytosolic N- and C-terminal domains and loops, which may bind to clathrin-coat adaptors, including AP-1 and AP-3 (Robinson and Bonifacino, 2001), and other adaptors, such as TIP47, PACS-1 (Rohn et al., 2000) or the retromer (Seaman, 2005). Our data suggest that mAtg9 behaves like the well-characterized CI-MPR, recycling between the TGN and the late endosome, thus escaping degradation in the lysosome. Under normal conditions the components and machinery involved in trafficking mAtg9 may be similar to those used for the CI-MPR. The ability of mAtg9 to recycle away from the late endosome/lysosome may be particularly important during starvation (see below).

The normal subcellular distribution of mAtg9 is also very similar to the distribution of WIPI-49 (Jeffries et al., 2004), a mammalian homologue of Atg18p (Barth et al., 2001; Guan et al., 2001), a cytosolic protein which binds phosphatidylinisitol (3)-monophosphate [PtdIns(3)*P*] (Jeffries et al., 2004; Reggiori et al., 2004). In mammalian cells, WIPI-49 overexpression perturbs the distribution of CI-MPR causing it to accumulate in the peri-nuclear region, suggesting it acts as a regulatory component. In *S. cerevisiae*, Atg18p and Atg9p interact in an Atg1p- and Atg2p-dependent manner (Reggiori et al., 2004). It is not known whether mAtg9 and WIPI-49 interact; however, we have observed a similar perturbation of CI-MPR localization following overexpression of mAtg9 (data not shown). This suggests that mAtg9 and WIPI-49 functions in the same transport step between the TGN and late endosomes.

Trafficking of mAtg9 after starvation

In *S. cerevisiae* Atg9 is required for autophagy and, therefore, it was anticipated the mammalian homologue is required for autophagy too. Indeed, data from Yamada et al. support this hypothesis because siRNA knockdown of ATG9L1 inhibited the appearance of GFP-LC3 spots after 24 hours starvation (Yamada et al., 2005). Our experiments analysed long-lived protein degradation and GFP-LC3-II appearance after mAtg9-depletion by siRNA, and further support the data of Yamada et al. (Yamada et al., 2005), although we did not observe a reproducible decrease in GFP-LC3 spots. The difference between these results may have to do with the long (24 hours) starvation used by Yamada and co-workers, and remains to be clarified. It has, however, been shown in yeast that there is not an absolute correlation between GFP-Atg8 on the PAS and the level of ScAtg8p-PE (the yeast equivalent of LC3-II), in

particular with regard to the phenotype of class C mutants, which includes ScATG9 (Suzuki et al., 2001). Another possible explanation for the lack of decrease in GFP-LC3 spots in our hands is that, like Atg5 (Hosokawa et al., 2006), only small amounts of mAtg9 may be required for AV formation and this small amount is present in siRNA-treated cells. This possibility can not be currently ruled out.

After starvation, mAtg9 colocalized with GFP-LC3 on both early AVis and late, Rab7-positive AVds. This was unexpected from the data in yeast, which show ScAtg9 is not on AVs accumulating in the vacuole (Lang et al., 2000; Noda et al., 2000), but is recycling from the PAS (Reggiori et al., 2004). Our data suggest that, if mAtg9 is recycled, it is recycled from the maturing AVs, probably before it becomes an autolysosome. Alternatively, some mAtg9 might remain on the AVd and be degraded in the autolysosome. Although we have found no evidence for degradation during induction of autophagy in primary rat hepatocytes, which exhibit a robust autophagic response (A.Y., unpublished observations), this requires further confirmation.

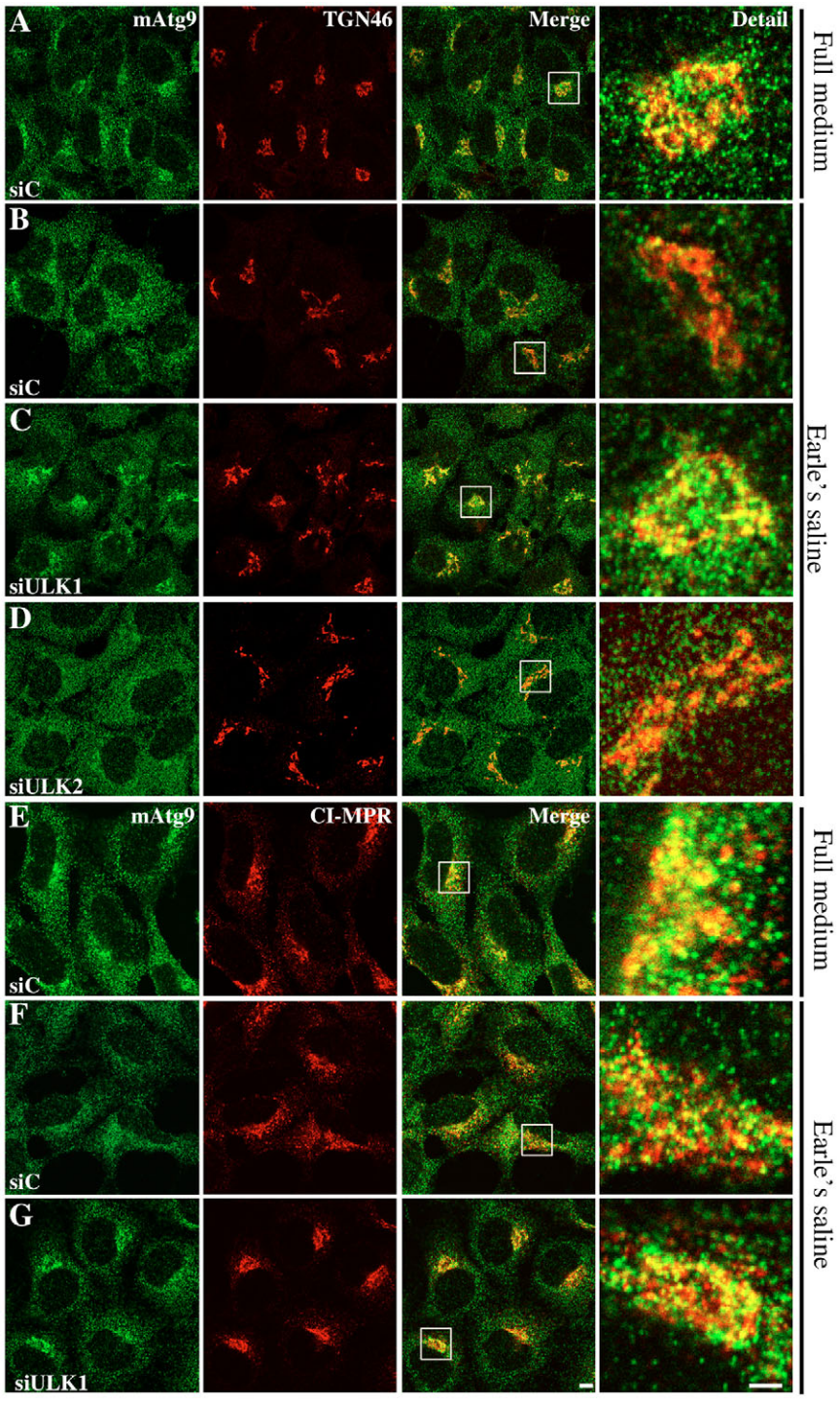

siRNA depletion of Atg1 but not Atg5, 6, or 7 affects mAtg9 localization

In *S. cerevisiae*, recycling of Atg9p from the PAS requires Atg1p, Atg2p, Atg18p and the autophagy-specific Vps34 PtdIns 3-kinase complex-I subunit Atg14p (Kihara et al., 2001b). Depletion of Atg1p and several other Atgs results in an accumulation of Atg9p at the PAS (Reggiori et al., 2004). Since we have shown after starvation and rapamycin treatment that the juxta-nuclear TGN population of mAtg9 redistributes in a reversible and amino-acid-sensitive manner, we tested the effect of depletion of ULK1 (the mammalian homologue of Atg1) (Yan et al., 1998) on the trafficking of mAtg9. SiRNA depletion of ULK1 resulted in a reproducible inhibition of the redistribution of mAtg9 to the peripheral pool, and an increase in the population of mAtg9 colocalized with TGN46.

Interestingly, depletion of the human homologues of Atg5, Beclin/Atg6 or Atg7 did not significantly inhibit mAtg9 redistribution in starved cells. In agreement with a previous genetic classification, it was anticipated that knockdown of both Atg5 and Atg12 would have no affect on Atg9 localization (Suzuki et al., 2001). However, deletion of Atg7 in *P. pastoris* has been shown to inhibit movement of PpAtg9 from the peri-vacuolar structures to the sequestering membranes (Chang et al., 2005). The difference between these and our results could be attributed to the unique nature of the membranes involved in the process of pexophagy, or a difference in the

Fig. 8. The starvation-induced dispersal of mAtg9 can be blocked by knockdown of ULK1 but not ULK2. HEK293 cells were treated with either control siRNA (A,B,E,F) or siRNA to either ULK1 (C,G) or ULK2 (D) and incubated in FM (A,E) or for 2 hours in ES medium (B-D,F,G). The cells were then fixed and labelled with antibodies against mAtg9 and TGN46 or CI-MPR. The starvation-induced dispersal of both mAtg9 (B,F) and CI-MPR (F) could be blocked by siRNA-mediated knockdown of ULK1 (C,G) but not ULK2 (D). Bars, 5 μm.

role of Atg9 in selective (pexophagy) autophagy versus non-selective macroautophagy. SiRNA depletion of Beclin1/Atg6 had only a minor affect on the starvation-induced redistribution of mAtg9. In mammalian cells, the type III PtdIns 3-kinase is required for autophagy (Petiot et al., 2000) and Beclin1 is a subunit of this complex (Kihara et al., 2001a). Recent data suggests this complex is required for autophagy but not other endosomal pathways requiring type III PtdIns 3-kinase (Zeng et al., 2006). There are several explanations for the lack of effect of Beclin1 depletion on mAtg9, including the possibility that the kinase activity of the type III PtdIns 3-kinase is not affected by Beclin1 depletion. In yeast, deletion of VPS30/Atg6 does not reduce the activity of PtdIns 3-kinase (Kihara et al., 2001a). By contrast, we observed a strong inhibition of the starvation-induced redistribution of mAtg9 with a PtdIns 3-kinase inhibitor. It has been shown that PtdIns 3-kinase is required for the exit of CI-MPR (Gaffet et al., 1997). Furthermore, it has been reported that there may be an inhibitor-sensitive endosomal trafficking step, involving CI-MPR, which is not mediated by type III PtdIns 3-kinase (Row et al., 2001). It remains to be clarified which PtdIns 3-kinase is involved in mAtg9 trafficking, and whether the effect of LY294002 on mAtg9 is related to its constitutive, endosomal cycling or starvation-induced trafficking.

Our data demonstrate that there is an alteration of TGN-to-endosome trafficking during starvation, which affects both mAtg9 and the CI-MPR. At present, we cannot distinguish whether the redistribution of mAtg9 reflects the role of mAtg9 in autophagy or a more general effect on membrane trafficking. Starvation of mammalian cells has been reported to attenuate secretion as a result of decreasing transport from the Golgi to the plasma membrane (Shorer et al., 2005). We also cannot exclude that ULK1 knockdown both in unstarved and starved cells results in accumulation of mAtg9 in a juxta-nuclear region because the target or acceptor downstream compartment is no longer available for delivery of mAtg9.

Conclusion

Since our data suggest the compartment on which the mAtg9 accumulates after depletion of mAtg1 is a juxta-nuclear TGN compartment, by analogy with the yeast model, this site of mAtg9 accumulation would, therefore, be the PAS or the phagophore. We have no data to support or exclude the possibility that this compartment represents the PAS and further data are required to characterize this juxta-nuclear membrane compartment. It is possible that inhibition of mAtg9 exit from the juxta-nuclear compartment results in a block in the delivery of mAtg9 to the PAS that is neither the TGN nor late endosomes, but a transient, and so far unidentified structure.

Our data indicate that inhibition of TGN exit correlates with the inhibition of autophagy and, therefore, we hypothesize that movement of mAtg9 from the TGN to endosomes is required for autophagy. More generally, our data imply a role for Golgi and endosomal trafficking in AV formation. In support of this, Noda et al. proposed that ScAtg9 marks the membrane to be donated to the AV, leading to the completion of the AV (Noda et al., 2000). Although we do not know whether mAtg9 has an identical function in mammalian cells, we speculate that the TGN-endosome pathway provides components for the production of an AV, and that this provision is mediated by mAtg9. Interestingly, it has been suggested that ScAtg9p self-aggregates and functions in delivery of membrane to the expanding PAS (Reggiori et al., 2005). Further progress towards understanding the role of mAtg9 in autophagy requires a better understanding of its function in both normal and starved cells.

Materials and Methods

Antibodies and reagents

Anti-mAtg9 peptide antibodies were raised in rabbits against the N- and C-terminal 20 amino acids, affinity purified using standard procedures, and conjugated to Alexa Fluor-488 or Alexa Fluor-555 for double-labelling experiments (Molecular Probes). Rabbit polyclonal: anti-CI-MPR was raised in house (Dittié et al., 1999). Anti-GFP, anti-Mannosidase II, anti-p58, anti-Rab7, and anti-Rab9 antibodies were kind gifts from T. Hunt (CRUK, London, UK), G. Warren (Yale University, New Haven, CT), J. Saraste (University of Bergen, Norway), A. Wadinger-Ness (University of New Mexico, Albuquerque, NM), and S. Pfeffer (Stanford University, CA), respectively. Commercial antibodies used were: anti-TGN46 (Serotec, UK), anti-actin (Sigma), anti-EEA1, anti-GM130 and anti-LAMP2 (BD Biosciences, USA), anti-HA (Covance, UK), anti-CI-MPR and anti-superoxide dismutase 1 (AbCam, UK), anti-PDI (StressGen, Canada), and anti-TGN38 (Affinity Bioreagents, USA).

Immunofluorescence

HEK293 or HEK293/GFP-LC3 stable (Köchl et al., 2006) cells were grown in Dulbecco's modified Eagle's medium (DMEM) 10% foetal calf serum (FCS), fixed using 3% paraformaldehyde (PFA), permeabilized using 0.2% Triton X-100, incubated with primary and subsequently secondary antibodies in 0.2% gelatin and mounted in Mowiol 4-88 (Calbiochem). Slides were examined using a confocal laser scanning microscope (LSM510; Carl Zeiss Inc.) equipped with a 63×/1.4NA plan-Apochromat oil immersion objective lens.

Preparation of endosomes from rat liver

Rat liver endosomes were prepared as described (Ellis et al., 1992), with the following modifications. The liver was perfused with perfusion buffer (PB; 142 mM NaCl, 6.7 mM KCl, 10 mM Hepes-NaOH pH 7.4) (Seglen, 1976) at 37°C, and HRP-biotin was added and recirculated through the liver for 10 minutes and then chased for 20 minutes with PB into late endosomes before homogenization as described.

Live cell imaging

Monomeric red fluorescent protein (mRFP; a gift from R. Tsien, Stanford, CA) fused to mAtg9 was used for live cell imaging. YFP-HLA-A2-CFP is a chimeric protein tagged on the lumenal face of the ER with YFP and on the cytosolic face with CFP (Lorenz et al., 2006). NRK cells were co-transfected with YFP-HLA-A2-CFP and mRFP-mAtg9 using Fugene (Roche). 18 hours post transfection cells were placed into KHM buffer (110 mM potassium acetate, 20 mM Hepes, 2 mM $MgCl_2$) and transferred to the microscope. Cells co-expressing YFP-HLA-A2-CFP and mRFP-mAtg9 were visually selected, and confocal imaging parameters were determined. The pre-image was captured, and digitonin added to a final concentration of 0.013% (w/v). After a 2-minute incubation, the post-digitonin image was captured. Trypsin was added to a final concentration of 0.005% and after a 5-minute incubation, the post-trypsin image was captured. All live cell images were captured using identical parameters.

RNAi

siRNA SMART pools or individual duplexes corresponding to ULK1 (NM_003365), Atg5 (NM_004849), Beclin1 (NM_003766), Atg7 (NM_006395) and Atg12 (NM_004707) were purchased from Dharmacon (USA). A single siRNA, sequence GUACAUGAAUUGCUUCUUG was used for mAtg9 (NM_024085) and is designated, ID2. A scrambled version, UACCUUUAGCAUGAUGUGU was used as control siRNA for mAtg9, designed using http://bioinfo.wistar.upenn.edu/siRNA/siRNA.htm. A non-targeting control Dharmacon SMART Pool was also used. siRNA was used at a final concentration of 25 nM and was transfected into HEK293 cells using Oligofectamine (Invitrogen) according to the manufacturer's instructions. Cells were incubated for 72 hours before manipulation.

Cryo-immunoelectron microscopy

Cryoimmunogold labelling was performed on HEK293 cells. Cells were fixed in 4% PFA in 0.1 M Sörensen's buffer (pH 7.4). and processed as previously described (Köchl et al., 2006). Cells were labelled with anti-GM130, mAtg9 and anti-CI-MPR followed by gold-conjugated secondary antibodies, or gold-conjugated protein A. To label endosomes, cultures were incubated with 6 nm BSA-gold for 2 hours prior to fixation.

In vivo glycosylation analysis

HEK293 cells were transfected using Lipofectamine 2000 (Invitrogen) with either mAtg9 HA tagged at the N-terminus (HAmAtg9), HAmAtg9/N99D,

HAmAtg9/N224D/N507D, or HAmAtg9/N99D/N224D/N507D. 16 hours after transfection, cells were homogenized and centrifuged at 2200 ***g*** for 10 minutes at 4°C. The resulting PNS was centrifuged at 45,000 rpm in a TLA45 rotor (Beckman) for 1 hour at 4°C. The pellet was resuspended in PBS, containing protease inhibitors [50 μg/ml Chymostatin, 0.5 μg/ml leupeptin, 50 μg/ml Antipain, 0.5 μg/ml pepstatin A (all Sigma) and 0.1 μg/ml Pefabloc (Roche)] and treated with glycosidase enzymes, EndoH or PNGaseF (New England Biolabs, USA). The samples were analysed by SDS-PAGE and western blotting. Samples for mAtg9 detection in SDS-sample buffer were not boiled.

In vitro topology analysis

In vitro synthesis was carried out essentially as described (Crawshaw et al., 2004). After the in vitro translation in the presence of microsomes, the reaction mix was loaded on a high-salt cushion [250 mM sucrose, 0.5 M KOAc, 5 mM $Mg(OAc)_2$, 50 mM HEPES KOH pH 7.9] and centrifuged at 55,000 rpm in a TLA100 rotor (Beckman) for 10 minutes at 4°C. The pellet was resuspended in low-salt cushion [50 mM sucrose, 100 mM KOAc, 5 mM $Mg(OAc)_2$, 50 mM Hepes KOH pH 7.9] and treated with either glycosidases or proteinase K in the presence or absence of Triton X-100, TCA precipitated, washed with acetone and resuspended in immunoprecipitation buffer (20 mM Tris-HCl pH 7.5, 150 mM NaCl, 5 mM EDTA, 0.3% Triton X-100). Samples were incubated with antibody overnight at 4°C, then with protein-A–Sepharose beads (GE Healthcare, UK) for at least 4 hours. Protein-A–Sepharose-bound material was washed, eluted with Laemmli sample buffer and analysed by SDS-PAGE and autoradiography.

Protein degradation assays

Protein degradation assays were carried out and analysed as described previously (Gronostajski and Pardee, 1984) with the following modifications. HEK293 cells were treated with siRNA oligonucleotides for 2 days. Cells were then placed in growth medium containing valine (65 μM) and [^{14}C]-valine (0.2 μCi/mL) and further incubated overnight. Cells were chased with full medium (FM) containing 2 mM valine for 4 hours, and then either incubated in Earle's medium (ES) or FM, containing 2 mM valine, for 2 hours. Aliquots of the medium were removed, the trichloroacetic acid (TCA)-soluble fraction was counted, and the cells were harvested and the TCA-insoluble fraction was counted.

We thank John Tooze, Giampietro Schiavo, and Grant Otto for discussions and critically reading the manuscript; J. Paul Luzio and Paul Prior for help and advice for the endosome preparation; Per Seglen and Franck Satre for help with the rat perfusion; and T. Jeffries for the GFP-Rab constructs.

References

Barbero, P., Bittova, L. and Pfeffer, S. R. (2002). Visualization of Rab9-mediated vesicle transport from endosomes to the trans-Golgi in living cells. *J. Cell Biol.* **156**, 511-518.

Barth, H., Meiling-Wesse, K., Epple, U. D. and Thumm, M. (2001). Autophagy and the cytoplasm to vacuole targeting pathway both require Aut10p. *FEBS Lett.* **508**, 23-28.

Blommaart, E. F., Krause, U., Schellens, J. P., Vreeling-Sindelarova, H. and Meijer, A. J. (1997). The phosphatidylinositol 3-kinase inhibitors wortmannin and LY294002 inhibit autophagy in isolated rat hepatocytes. *Eur. J. Biochem.* **243**, 240-246.

Bonifacino, J. S. and Traub, L. M. (2003). Signals for sorting of transmembrane proteins to endosomes and lysosomes. *Annu. Rev. Biochem.* **72**, 395-447.

Chang, T., Schroder, L. A., Thomson, J. M., Klocman, A. S., Tomasini, A. J., Stromhaug, P. E. and Dunn, W. A., Jr (2005). PpATG9 encodes a novel membrane protein that traffics to vacuolar membranes, which sequester peroxisomes during pexophagy in pichia pastoris. *Mol. Biol. Cell* **16**, 4941-4953.

Crawshaw, S. G., Martoglio, B., Meacock, S. L. and High, S. (2004). A misassembled transmembrane domain of a polytopic protein associates with signal peptide peptidase. *Biochem. J.* **384**, 9-17.

Dittié, A. S., Klumperman, J. and Tooze, S. A. (1999). Differential distribution of mannose-6-phosphate receptors and furin in immature secretory granules. *J. Cell Sci.* **112**, 3955-3966.

Dunn, W. A., Jr (1990). Studies on the mechanisms of autophagy: formation of the autophagic vacuole. *J. Cell Biol.* **110**, 1923-1933.

Ellis, J., Jackman, M., Perez, J., Mullock, B. and Luzio, J. (1992). Membrane traffic pathways in polarised epithelial cells. In *Protein Targeting: A Practical Approach* (ed. A. I. Magee and T. Wileman), pp. 25-57. Washington: IRL Press.

Ericsson, J. L. E. (1969). Studies on induced cellular autophagy II. Characterization of the membranes bordering autophagosomes in parenchymal liver cells. *Exp. Cell Res.* **56**, 393-405.

Gaffet, P., Jones, A. T. and Clague, M. J. (1997). Inhibition of calcium-independent mannose 6-phosphate receptor incorporation into trans-golgi network-derived clathrin-coated vesicles by wortmannin. *J. Biol. Chem.* **272**, 24170-24175.

Goud, B., Zahraoui, A., Tavitian, A. and Saraste, J. (1990). Small GTP-binding protein associated with Golgi cisternae. *Nature* **345**, 553-556.

Gronostajski, R. M. and Pardee, A. B. (1984). Protein degradation in 3T3 cells and tumorigenic transformed 3T3 cells. *J. Cell Physiol.* **119**, 127-132.

Guan, J., Stromhaug, P. E., George, M. D., Habibzadegah-Tari, P., Bevan, A., Dunn, W. A., Jr and Klionsky, D. J. (2001). Cvt18/Gsa12 is required for cytoplasm-to-vacuole transport, pexophagy, and autophagy in saccharomyces cerevisiae and pichia pastoris. *Mol. Biol. Cell* **12**, 3821-3838.

Gutierrez, M. G., Munafo, D. B., Beron, W. and Colombo, M. I. (2004). Rab7 is required for the normal progression of the autophagic pathway in mammalian cells. *J. Cell Sci.* **117**, 2687-2697.

Hosokawa, N., Hara, Y. and Mizushima, N. (2006). Generation of cell lines with tetracycline-regulated autophagy and a role for autophagy in controlling cell size. *FEBS Lett.* **580**, 2623-2629.

Jager, S., Bucci, C., Tanida, I., Ueno, T., Kominami, E., Saftig, P. and Eskelinen, E.-L. (2004). Role for Rab7 in maturation of late autophagic vacuoles. *J. Cell Sci.* **117**, 4837-4848.

Jeffries, T. R., Dove, S. K., Michell, R. H. and Parker, P. J. (2004). PtdIns-specific MPR Pathway association of a novel WD40 repeat protein, WIPI49. *Mol. Biol. Cell* **15**, 2652-2663.

Kihara, A., Kabeya, Y., Ohsumi, Y. and Yoshimori, T. (2001a). Beclin-phosphatidylinositol 3-kinase complex functions at the trans-Golgi network. *EMBO Rep.* **2**, 330-335.

Kihara, A., Noda, T., Ishihara, N. and Ohsumi, Y. (2001b). Two distinct Vps34 phosphatidylinositol 3-kinase complexes function in autophagy and carboxypeptidase Y sorting in saccharomyces cerevisiae. *J. Cell Biol.* **152**, 519-530.

Kim, J., Huang, W. P., Stromhaug, P. E. and Klionsky, D. J. (2002). Convergence of multiple autophagy and cytoplasm to vacuole targeting components to a perivacuolar membrane compartment prior to de novo vesicle formation. *J. Biol. Chem.* **277**, 763-773.

Klionsky, D. J. (2005). Autophagy. *Curr. Biol.* **15**, R282-R283.

Klionsky, D. J., Cregg, J. M., Dunn, W. A., Emr, S. D., Sakai, Y., Sandoval, I. V., Sibirny, A., Subramani, S., Thumm, M., Veenhuis, M. et al. (2003). A unified nomenclature for yeast autophagy-related genes. *Dev. Cell* **5**, 539-545.

Köchl, R., Hu, X., Chan, E. and Tooze, S. A. (2006). Microtubules facilitate autophagosomal formation and fusion of autophagosomes with endosomes. *Traffic* **7**, 129-145.

Lang, T., Reiche, S., Straub, M., Bredschneider, M. and Thumm, M. (2000). Autophagy and the cvt pathway both depend on AUT9. *J. Bacteriol.* **182**, 2125-2133.

Locke, M. and Sykes, A. K. (1975). The role of the Golgi complex in the isolation and digestion of organelles. *Tissue Cell* **7**, 143-158.

Lorenz, H., Hailey, D. W. and Lippincott-Schwartz, J. (2006). Fluorescence protease protection of GFP chimeras to reveal protein topology and subcellular localization. *Nat. Methods* **3**, 205-210.

Mizushima, N. (2004). Methods for monitoring autophagy. *Int. J. Biochem. Cell Biol.* **36**, 2491-2502.

Mizushima, N., Yamamoto, A., Hatano, M., Kobayashi, Y., Kabeya, Y., Suzuki, K., Tokuhisa, T., Ohsumi, Y. and Yoshimori, T. (2001). Dissection of autophagosome formation using Apg5-deficient mouse embryonic stem cells. *J. Cell Biol.* **152**, 657-668.

Nakamura, N., Rabouille, C., Watson, R., Nilsson, T., Hui, N., Slusarewicz, P., Kreis, T. and Warren, G. (1995). Characterization of a cis-Golgi matrix protein, GM130. *J. Cell Biol.* **131**, 1715-1726.

Noda, T. and Ohsumi, Y. (1998). Tor, a phosphatidylinositol kinase homologue, controls autophagy in yeast. *J. Biol. Chem.* **273**, 3963-3966.

Noda, T., Kim, J., Huang, W. P., Baba, M., Tokunaga, C., Ohsumi, Y. and Klionsky, D. J. (2000). Apg9p/Cvt7p is an integral membrane protein required for transport vesicle formation in the Cvt and autophagy pathways. *J. Cell Biol.* **148**, 465-480.

Novikoff, A. B. and Shin, W. Y. (1978). Endoplasmic reticulum and autophagy in rat hepatocyte. *Proc. Natl. Acad. Sci. USA* **75**, 5039-5042.

Petiot, A., Ogier-Denis, E., Blommaart, E. F., Meijer, A. J. and Codogno, P. (2000). Distinct classes of phosphatidylinositol 3′-kinases are involved in signaling pathways that control macroautophagy in HT-29 cells. *J. Biol. Chem.* **275**, 992-998.

Reggiori, F., Tucker, K. A., Stromhaug, P. E. and Klionsky, D. J. (2004). The Atg1-Atg13 complex regulates Atg9 and Atg23 retrieval transport from the pre-autophagosomal structure. *Dev. Cell* **6**, 79-90.

Reggiori, F., Shintani, T., Nair, U. and Klionsky, D. J. (2005). Atg9 cycles between mitochondria and the pre-autophagosomal structure in yeast. *Autophagy* **1**, 101-109.

Robb, G. B., Carson, A. R., Tai, S. C., Fish, J. E., Singh, S., Yamada, T., Scherer, S. W., Nakabayashi, K. and Marsden, P. A. (2004). Post-transcriptional regulation of endothelial nitric-oxide synthase by an overlapping antisense mRNA transcript. *J. Biol. Chem.* **279**, 37982-37996.

Robinson, M. S. and Bonifacino, J. S. (2001). Adaptor-related proteins. *Curr. Opin. Cell Biol.* **13**, 444-453.

Rohn, W. M., Rouille, Y., Waguri, S. and Hoflack, B. (2000). Bi-directional trafficking between the trans-Golgi network and the endosomal/lysosomal system. *J. Cell Sci.* **113**, 2093-2101.

Row, P., Reaves, B., Domin, J., Luzio, J. and Davidson, H. W. (2001). Overexpression of a rat kinase-deficient phosphoinositide 3-kinase, Vps34p, inhibits cathepsin D maturation. *Biochem. J.* **353**, 655-661.

Seaman, M. N. (2005). Recycle your receptors with retromer. *Trends Cell Biol.* **15**, 68-75.

Seglen, P. O. (1976). Preparation of isolated rat liver cells. *Methods Cell Biol.* **13**, 29-83.

Seglen, P. O., Gordon, P. B. and Holen, I. (1990). Non-selective autophagy. *Semin. Cell Biol.* **1**, 441-448.

Shorer, H., Amar, N., Meerson, A. and Elazar, Z. (2005). Modulation of N-ethylmaleimide-sensitive factor activity upon amino acid deprivation. *J. Biol. Chem.* **280**, 16219-16226.

Slusarewicz, P., Hui, N. and Warren, G. (1994). Purification of rat liver Golgi stacks. In *Cell Biology: A laboratory Handbook* (ed. J. E. Celis), pp. 509-517. Orlando, FL: Academic Press.

Sonnichsen, B., De Renzis, S., Nielsen, E., Rietdorf, J. and Zerial, M. (2000). Distinct membrane domains on endosomes in the recycling pathway visualized by multicolor imaging of Rab4, Rab5, and Rab11. *J. Cell Biol.* **149**, 901-914.

Suzuki, K., Kirisako, T., Kamada, Y., Mizushima, N., Noda, T. and Ohsumi, Y. (2001). The pre-autophagosomal structure organized by concerted functions of APG genes is essential for autophagosome formation. *EMBO J.* **20**, 5971-5981.

Thumm, M., Egner, R., Koch, B., Schlumpberger, M., Straub, M., Veenhuis, M. and Wolf, D. H. (1994). Isolation of autophagocytosis mutants of Saccharomyces cerevisiae. *FEBS Lett.* **349**, 275-280.

Tsukada, M. and Ohsumi, Y. (1993). Isolation and characterization of autophagy-defective mutants of Saccharomyces cerevisiae. *FEBS Lett.* **333**, 169-174.

Turner, R. and Tartakoff, A. (1989). The response of the Golgi complex to microtubule alterations: the roles of metabolic energy and membrane traffic in Golgi complex organization. *J. Cell Biol.* **109**, 2081-2088.

Ueda, T., Takeyama, Y., Ohmori, T., Ohyanagi, H., Saitoh, Y. and Takai, Y. (1991). Purification and characterization from rat liver cytosol of a GDP dissociation inhibitor (GDI) for liver 24K G, a ras p21-like GTP-binding protein, with properties similar to those of smg p25A GDI. *Biochemistry* **30**, 909-917.

Yamada, T., Carson, A. R., Caniggia, I., Umebayashi, K., Yoshimori, T., Nakabayashi, K. and Scherer, S. W. (2005). Endothelial nitric-oxide synthase antisense (NOS3AS) gene encodes an autophagy-related protein (APG9-like2) highly expressed in trophoblast. *J. Biol. Chem.* **280**, 18283-18290.

Yamamoto, A., Masaki, R. and Tashiro, Y. (1990). Characterization of the isolation membranes and the limiting membranes of autophagosomes in rat hepatocytes by lectin cytochemistry. *J. Histochem. Cytochem.* **38**, 573-580.

Yan, J., Kuroyanagi, H., Kuroiwa, A., Matsuda, Y.-I., Tokumitsu, H., Tomoda, T., Shirasawa, T. and Muramatsu, M.-A. (1998). Identification of mouse ULK1, a novel protein kinase structurally related to C. elegans UNC-51. *Biochem. Biophys. Res. Commun.* **246**, 222-227.

Zeng, X., Overmeyer, J. H. and Maltese, W. A. (2006). Functional specificity of the mammalian Beclin-Vps34 PI 3-kinase complex in macroautophagy versus endocytosis and lysosomal enzyme trafficking. *J. Cell Sci.* **119**, 259-270.

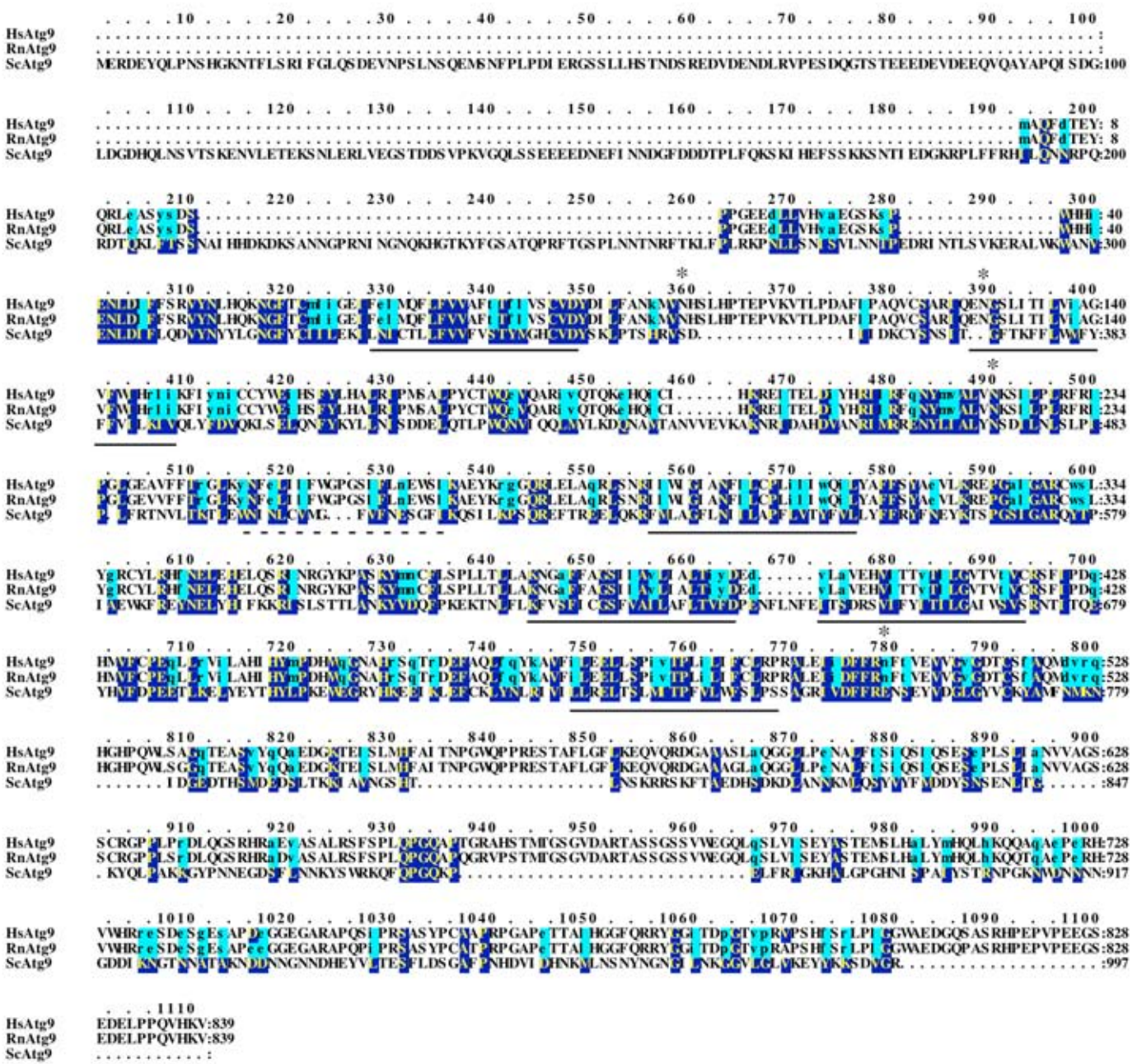

Fig. S1A. Sequence alignment of *Saccharomyces cerevisiae* (Sc) versus human (Hs – *Homo sapiens*) and rat (Rn - *Rattus norvegicus*) Atg9. Sequences were aligned using ClustalX and displayed using MacBoxShade. Residues in the yeast sequence which are conserved in the human and rat sequences are in yellow text on a dark blue background. Similar residues are in lower case on a light blue background. Potential N-glycosylation sites in the human and rat sequences are marked with asterisks. Potential transmembrane domains are underlined.

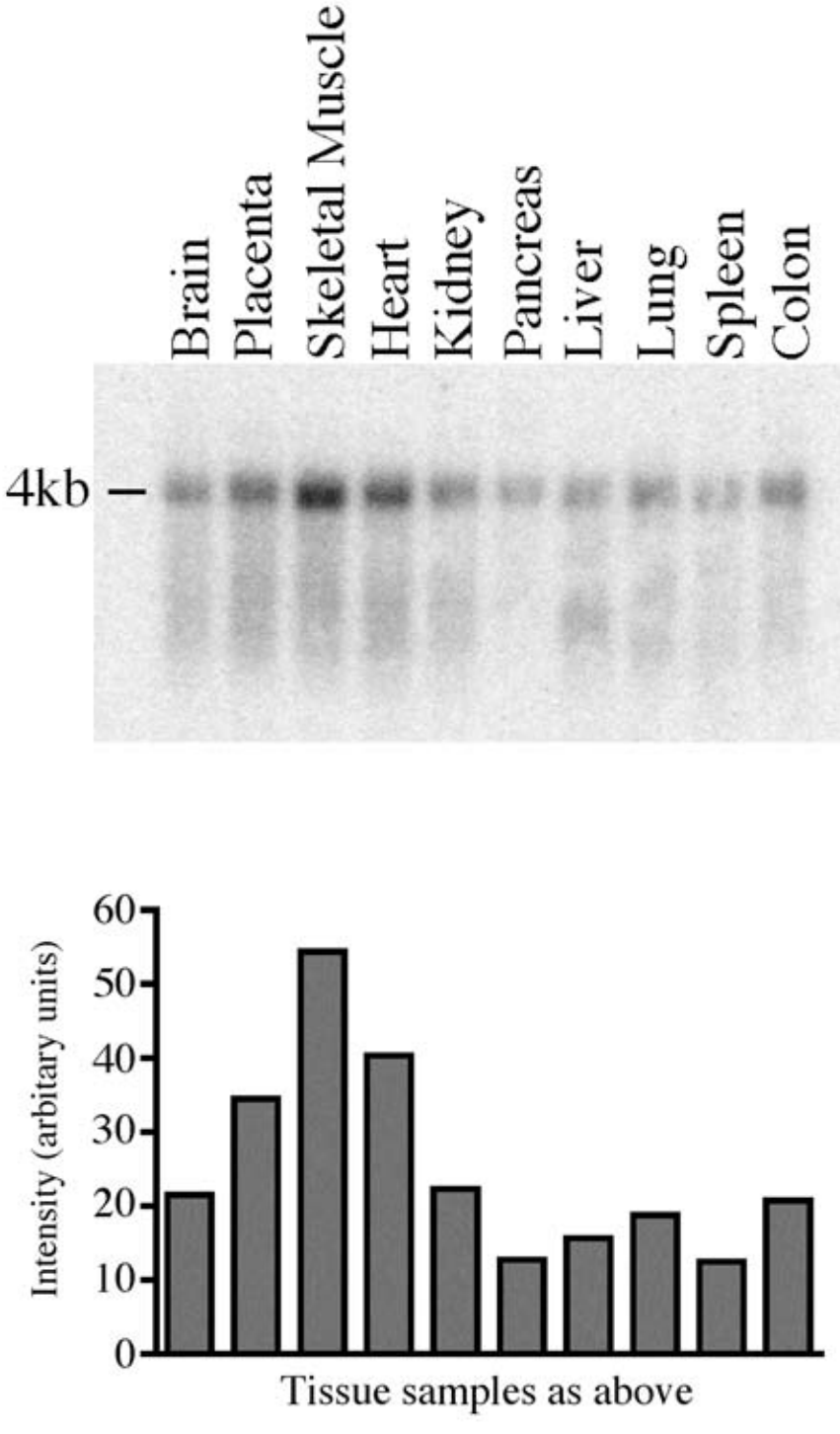

Fig. S1B. *mAtg9 transcript levels*. A poly-A Northern blot, purchased from Ambion, was probed with a template corresponding to the 3' end of the HsATG9 open reading frame. Including UTRs the HsATG9 cDNA is ~3.8kb. The blot was tested by the manufacturer for equal loading.

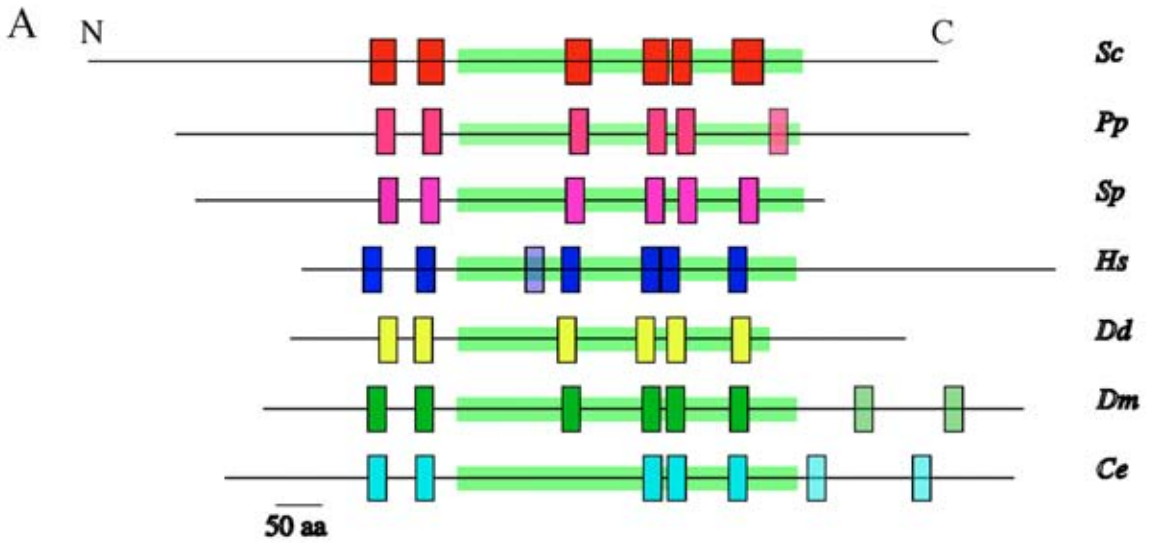

B

Candidate membrane-spanning segments:

	TM #	AA #	Score
Certain	1	68- 88	1.9146
Certain	2	128- 148	1.4281
Putative	3	249- 269	0.7719
Certain	4	290- 310	1.7687
Certain	5	378- 398	1.8125
Certain	6	401- 421	1.2125
Certain	7	476- 496	1.1000

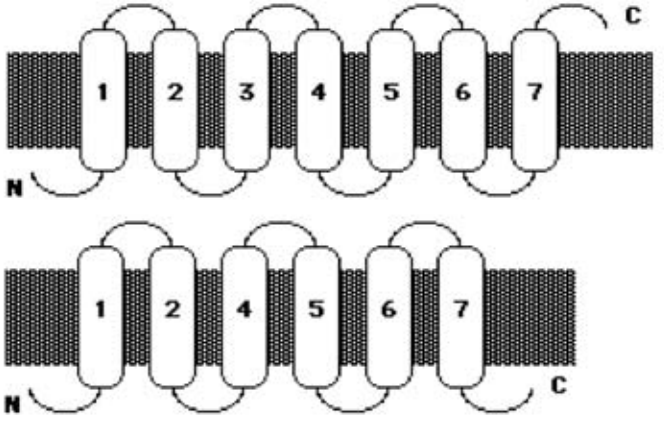

Fig. S2. *mAtg9 topology*. (**A**) When the Atg9 homologues from various species are aligned together, a similarity is seen in the spacing between the transmembrane (TM) domains which are represented by coloured boxes in the diagrams, with paler TMs being putative. The green block in each diagram represents the conserved Atg9 domain from Pfam. *Sc* = *S. cerevisiae*, *Pp* = *P. pastoris*, *Sp* = *S. pombe*, *Hs* = *H. sapiens*, *Dd* = *D. discoideum*, *Dm* = *D. melanogaster*, *Ce* = *C. elegans* (GenBank Accession Nos. NP_010132, AAL77196, CAA20482, NP_076990, AAO39079, AAF58018 and AAC69227, respectively). (**B**) Position of the predicted TMs in mAtg9 and models with six or seven TM domains. Topology predicted by TopPredII.

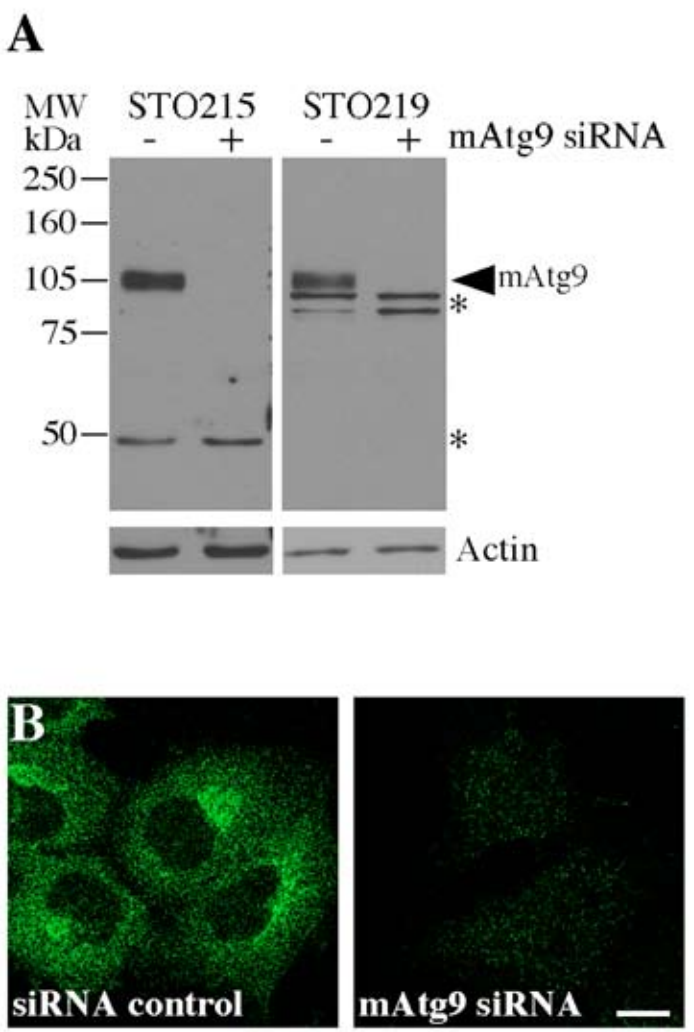

Fig S3. *Specificity of the mAtg9 antibodies.* (**A**) HEK293 cells were treated with either control or mAtg9 specific siRNA oligonucleotides for 72h before extraction. Subsequent Western blots were probed with the mAtg9 N- and C-terminal specific antibodies STO215 and STO219 respectively (* marks non-specific bands). (**B**) Cells treated in parallel were fixed for immunofluorescence and labelled with STO219. Bar = 10μm.

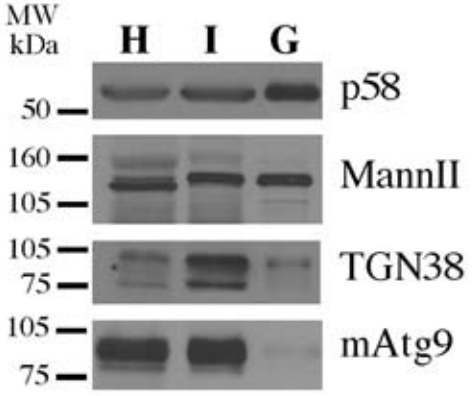

Fig. S4. *Rat liver Golgi preparation*. To corroborate the immunofluorescence data showing mAtg9's presence on TGN membranes, Golgi membranes were purified from rat liver as described previously (Slusarewicz et al., 1994). Note that TGN membranes are largely separated from Golgi membranes by this stacked Golgi fractionation procedure, being only present at 10-15% of their original level (Nakamura et al., 1995). Aliquots of the homogenate (H), the intermediate fraction (I) (crude Golgi membranes) and the purified Golgi-stacked cisternae (G) were probed with antibodies to p58, mannosidase II (Mann II), TGN38 (rat equivalent of TGN46) and mAtg9.

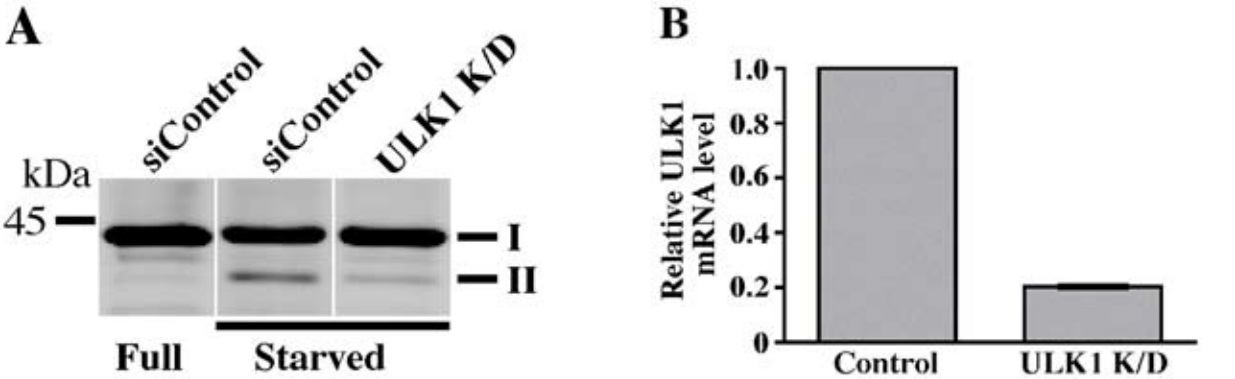

Fig. S5. *siRNA depletion of ULK1 inhibits the formation of lipidated GFP-LC3-II upon starvation.* (**A**) HEK293 cells stably expressing GFP-LC3 were treated with either control or ULK1 specific siRNA oligonucletides 72h before extraction. GFP-LC3 was detected using an anti-GFP antibody. (**B**) Quantitation by RT-PCR of mRNA levels in ULK1 siRNA treated cells relative to the control siRNA treated cells. Total RNA was purified from cells using RNeasy mini kit (Qiagen). cDNA was reverse transcribed using the Superscript II kit (Invitrogen) and amplified using ULK1 primers (AGATGTTCCAGCACCGTGAG; ACAGCTTGCACTTGGTGACG) and B-Actin (normalizing control) (AGACCTGTACGCCAACACAG; AGGAGGAGCAATGATCTTG). mRNA was quantified using the MJ Research (USA) Chromo4 Real Time PCR system and SYBR Green (Applied Biosystems, USA). Fold changes in ULK1 mRNA levels are normalized to Actin.